Supplementary Appendix

Table of Contents

Supplementary Methods

The Index Family
In the index family, six cases of histopathologically-confirmed multinodular goiters (MNGs) occurred with 3 cases of histopathologically-confirmed schwannomas and 2 cases of imaging-confirmed schwannomas:

First generation: In the 85-year old grandfather (I-1) a MNG was diagnosed and partial thyroidectomy was performed at the age of 29 followed by a total thyroidectomy at 47 y/o. A schwannoma of the pinna was diagnosed 33 years later (70 y/o).

Second Generation: The proband (II-1) was also diagnosed with a MNG for which he had a total thyroidectomy at the age of 18. Ten years later a colloid goiter regrowth prompted a total thyroidectomy (details are provided in Figure 1). Person II-2 had a MNG, a mature cystic teratoma, multiple peripheral schwannomas (9 up to date), a mature cystic teratoma and an ovarian serous cystadenofibroma in the contralateral ovary. She had a total thyroidectomy when she was 20 years old and over the next 18.5 years had a midline neck regrowth exhibiting solid and cystic nodular thyroid tissue. At the age of 49, she had a complete thyroidectomy. This patient also had a right salpingo-oophorectomy at the age of 18 to excise the mature cystic teratoma and later had a left salpingo-oophorectomy at age 26 to excise the ovarian serous cystadenofibroma. The archival tissue from the ovarian tumors did not pass quality requirements for genomic analysis. Person II-2 was diagnosed with a schwannoma around her left femoral nerve and underwent surgeries at the ages of 20 and 23 to get it excised. At 43 years old, she underwent surgery to excise a schwannoma located in the right axilla. She was again diagnosed with three schwannomas in her left foot and a single schwannoma around the right common peroneal nerve at the age of 54, for which she underwent surgery at the same age to have them all excised. Early in 2018, she was diagnosed with 3 schwannomas in the neck region (Supplementary Figure 1).

Third generation: Patients III-1, III-2 and III-3 each had a total thyroidectomy at the ages of 23, 18 and 21, respectively. III-1was diagnosed with a form of autism and also had brain surgery at the age of 7 years to excise a choroid plexus papilloma (WHO I). III-1 and III-3 were diagnosed with multiple schwannomas. III-1 was diagnosed at the age of 25 with three schwannomas located in the left elbow region that could have been present for some years. III-3 was diagnosed at the age of 23 with two schwannomas: one in the left wrist and one in the right shoulder that also could have been present for some years and were both excised a year and a half later. III-2 was diagnosed at the age of 27 with a single schwannoma located in the right knee and resected one year later. Individual III-4 died from a car accident at the age of 17 years old.

Schwannoma symptomatology: Individual III-1 showed signs of intense pain to palpation of his schwannoma. Since we first identified these familial schwannomas, family members are refering discomfort, tenderness and paresthesias localized to the tumor and radiating along nerve of origin although no individuals complained of overt pain related to their schwannomas.

DNA isolation
Germline DNA from members of the index family (n = 9) and from cases of MNGs with a suspected hereditary origin (n = 18) was isolated from blood using Gentra Puregene Blood kit (Qiagen, California, USA) following the manufacturer's instructions. Tumor DNA from fresh frozen samples (n = 7) was isolated with DNeasy Blood and Tissue Qiagen kits (Qiagen, California, USA). Tumor DNA from sporadic CPT cases (n = 74), schwannoma cases (n = 181)

and family 1 cases (n = 7) was isolated from formalin-fixed, parrafin-embedded (FFPE) material using the Maxwell 16 FFPE tissue RSC DNA purification Kit (Promega, Wisconsin, USA) in accordance with the manufacturer's protocol. DNA from 315 thyroid cancer and 106 benign nodules was extracted from fine needle aspiration (FNA) biopsies using QIAamp DNA Mini Kit (Qiagen, Hilden, Germany).

Linkage analysis to 14q
Polymorphic microsatellite repeat markers located at 14q32 (D14S1010, D14S267, D14S62, D14S1455, D14S265, D14S1030, D14S1054 and D14S274) were used for haplotype analysis as described by Rudkin and colleagues(1).

MLPA assay
We screened the germline of the proband and of the 18 familial MNGs for deletions or duplications of *DICER1* using an in-house multiplex ligation-dependent probe amplification (MLPA) assay, as described previously(2).

DICER1 screening
Germline DNA from the index family was screened for the full *DICER1* coding region and exon–intron boundaries in germline DNA from the index family using a custom Fluidigm Access Array (Fluidigm, California, USA) which targets all exons and exon-intron boundaries of *DICER1*, as previously described(3).

Variant calling in germline samples subjected to whole exome sequencing (WES)
Bioinformatics analysis of exome sequencing data was performed using our WES pipeline as previously described(4). Briefly, our pipeline uses Trimmomatic (v.0.35) and BWA (v. 0.5.9) to trim and align sequenced reads to the reference genome (hg19); GATK and Picard (http://broadinstitute.github.io/picard//) to perform local realignment around small insertions and deletions (indels) and to mark read duplicates, respectively.
Next, GATK was applied to assess capture efficiency and coverage for all samples. A mean coverage of 139-fold (ranging from 90-238-fold) was obtained for all consensus coding sequence (CCDS) in germline samples and 98% and 97% of CCDS bases were covered by at least 5 and 20 reads, respectively (Supplementary Table 1).
Single nucleotide variants (SNVs) and indels were called using Samtools and subsequently annotated by ANNOVAR(5). Those variants which most likely damage the protein (nonsense, canonical splice-site, coding indels and missenses were considered for further analysis. To remove common variants and false positive calls, candidate mutations were subjected to several filtering steps and eliminated if they fulfilled any one of the following criteria: (i) genomic position of variant covered by <5-reads, (ii) <5 reads supported the alternative variant, (iii) variant had allelic ratio <10% for SNVs or <15% for indels, (iv) variant had allele frequency >0.001 in NoTCGA-ExAC databases (release 0.3 2016-01-13), or seen as homozygote in ExAC database (release 0.3 2016-01-13) (v) missense variants that were not predicted to be disease causing by 3 out of 6 bioinformatic algorithms (SIFT, PolyPhen, MutationTaster, Revel, MCAP and CADD)(6-11). Finally, The Integrative Genomics Viewer was used for the manual examination and visualization of all potential candidate variants(12).

Variant calling in somatic samples subjected to WES
Bioinformatics analysis of exome sequencing data was performed using our WES pipeline as described above. GATK was applied to assess capture efficiency and coverage for all samples. A mean coverage of 161-fold (ranging from 93-196-fold) was obtained for all consensus coding sequence (CCDS) in samples and 98 % and 96% of CCDS bases were covered by at least 5 and 20 reads, respectively (Supplementary Table 2).

Potential somatic substitutions, single nucleotide variants (SNVs) and indels, were called using Mutect (see https://confluence.broadinstitute.org/display/CGATools/MuTect for method) and IndelLocator (see https://confluence.broadinstitute.org/display/CGATools/Indelocator for methods) on the basis of BWA alignments and were then annotated with ANNOVAR(5). Those variants most likely to damage the protein (nonsense, canonical splice-site, coding indels and missense) were considered for further analysis. To remove common variants and false positive sequencing artifacts, candidate somatic mutations were subjected to several filtering steps and eliminated if they fulfilled any one of the following criteria: (i) genomic position of variant covered by <5-reads, (ii) <5 reads support the alternative variant, (iii) variant has allelic ratio <10% for SNVs or <15% for indels, (iv) variant has allele frequency >0.001 in TCGA-ExAC databases (release 0.3 2016-01-13) or seen as homozygote in ExAC database (build). (v) missense variants that were not predicted to be disease causing by 3 out of 6 bioinformatic algorithms (SIFT, PolyPhen, MutationTaster, Revel, MCAP and CADD)(6-11). Finally, The Integrative Genomics Viewer was used for the manual examination and visualization of all potential candidate variants(12).

RNA seq analysis and normalization
MicroRNA libraries were sequenced using Illumina HiSeq 2500 with 50-bp read length. Adapters and low quality bases were trimmed using cutadapt(13) and trimmed reads with length >16 were kept. The average high quality read counts were 34M (ranging from 21M to 51M). For quality control, FASTQC (version v0.11.5)(14) was run on all samples. Reads were mapped to the human genome (hg19) using the bowtie version 1.1.2(15). The feature Counts tool from the Subread(16) was used to generate counts of reads mapped to the mature miRNA of miRBase (v20 with genome-build GRCh37.p5). Counts for each sample were combined and loaded into the R statistical environment (https://cran.r-project.org, version 3.4.3). Differential analysis was performed using various packages from the Bioconductor project(17), including edgR(18) and LIMMA(19). Briefly, transcripts with low counts were filtered by a counts per million (CPM) cutoff. The cutoff value was determined by finding the CPM (minimum 10 reads, across at least 4 samples). The data was normalized for sequencing depth using the weighted Trimmed Mean of M-values method as implemented in the calcNormFactors function of the edgR (method = TMM). Then logCPM transformation and mean-variance relationship estimation was performed using the VOOM function of limma package(19). Differential expression analysis was conducted by linear modelling on the normalized data for the comparison in question (group effect = the *DGCR8* mutation). Empirical Bayes moderation was applied, which gives a more precise estimation of gene-wise variability (eBayes function of limma).

The same analysis was performed on pre-miRNA raw reads with two differences. Adapters and low quality bases were trimmed using cutadapt(13) and trimmed reads with length >30 were kept. The average high quality read counts were 130M (ranging from 97M to 232M). In addition, the cutoff for the low counts transcripts was a minimum of 1 read, across at least 4 samples. Total RNA libraries were sequenced using Illumina HiSeq 4000 with paired-end 100-bp read length. Adapters and low quality bases were trimmed using Trimmomatic(21). The trimmed reads were aligned to the reference genome (hg19) using STAR in a two-passes approach. The average properly aligned paired reads was 125M (93M to 152M). The counts of read pairs overlapping genes was determined using htseq-count (22), with low counts filtered by a CPM cutoff (minimum 10 reads, across 4 samples). VOOM normalization was performed(20) and a linear model was applied on the normalized data for the comparison in question. Differential

analysis statistics were computed using moderated t-statistics as implemented in the LIMMA package(19).

Consensus Clustering

Unsupervised consensus clustering was performed in order to evaluate the clustering of DGCR8-mutant samples and their wild type counterparts (n sample = 33), based on their normalized miRNA profile, using the ConsensusClusterPlus R package(23). The clustering was evaluated for 2 up to 5 clusters (k = 2 to 5), with 1000 repetitions. Consensus distributions for each k is shown using empirical Cumulative Distribution Function (CDF) plot (Supplementary Figure 8A). As the CDF plot clearly shows, the 2-cluster solution performs best with lowest Proportion of Ambiguous Clustering (PAC). Consensus membership matrix for 2-cluster solution (k = 2) is shown using a heatmap in Supplementary Figure 8B. ConsensusClusterPlus was run with default parameters and minor modifications as followings: number of resampling = 1000; pItem = 0.8 (resampling for samples); clusterAlg= 'hc' (heirarchical, hclust algorithm);maxK = 5 (maximum cluster number to evaluate); pFeature = 0.8 (Proportion of miRNA to sample); The normalization of miRNA values was performed as explained above for differential expression analysis. In addition, as clustering performed on samples from public data as well as our data (Wilms and Schwannoma; n smaple = 24 and 9 respectively), data was also normalized for this effect using the removeBatchEffect function in the R limma package.

Gene Set Enrichment Analysis (GSEA)

We performed Gene Set Enrichment Analysis(24), based on comparison between DGCR8-mutated and wild type schwannomas, using 50 Hallmark Gene Sets(25). We reported the gene sets with FDR less than 0.01 (NES > 1.9 or NES < -1.9). This led to 5 significantly enriched gene sets (out of 50). Results are shown in Supplementary Figure 15 and Supplementary Table 13.

Supplementary Figures
Supplementary Figure 1. Magnetic Resonance imaging of the schwannomas in the index family
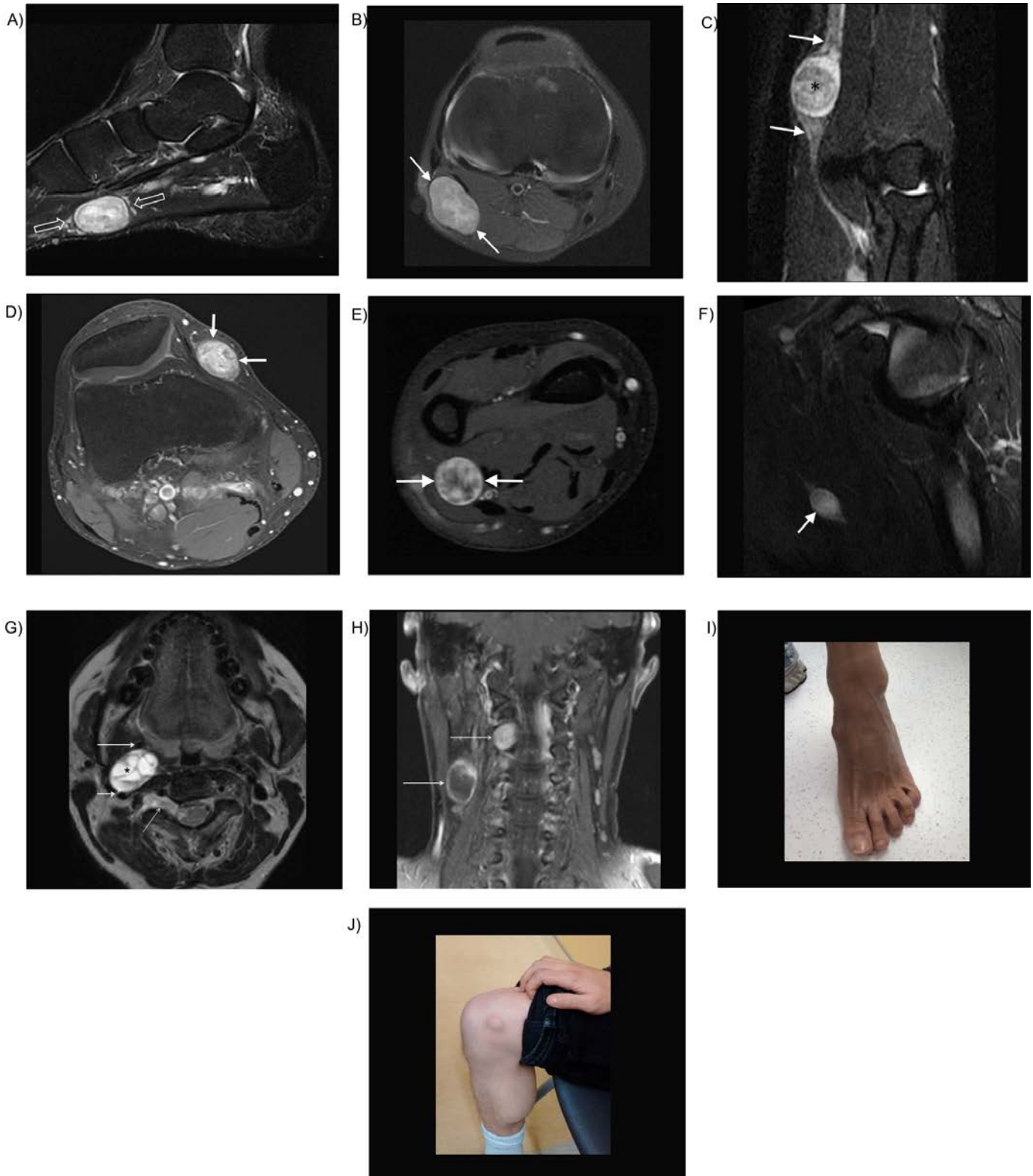
Supplementary Figure 1. (**A**) Sagittal STIR image shows an ovoid, heterogeneous mass in the distribution of the posterior tibial nerve. The lesion demonstrates a hyper intense rim, which is not specific, but which can be seen in the setting of schwannoma (open arrows) from a 54 year old female with schwannomas (II-2). (**B**) Axial fat-saturated proton density image at the knee in the same patient shows a heterogeneously hyper intense mass at the posterolateral knee in the region of the common peroneal nerve (white arrows) from a 54 year old female with schwannomas (II-2). (**C**) 25 year old male with schwannoma along the median nerve: Coronal Short Tau Inversion Recovery (STIR) image shows a well-circumscribed, heterogeneous mass (asterisk). Note the slightly eccentric relationship to the median nerve (white arrows) from III-1. (**D**) 27 year old male with schwannoma: Axial T1 fat-saturated image post contrast shows an ovoid, heterogeneously enhancing mass at the anteromedial knee (white arrows) from III-2. (**E**) Oblique sagittal STIR image demonstrates a fusiform high-signal mass within the right pectoralis major muscle (arrow) from 23 year old female with schwannoma III-3. (**F**) T1 fat-saturated image post contrast in the same patient at the level of the wrist demonstrates a heterogeneous, well marginated mass in the volar soft tissues medially (arrows). The lesion shows heterogeneous enhancement from 23 year old female (III.3) with schwannoma. (**G**) Axial T2-weighted image from a 56 year old female with schwannomas (II-2) demonstrates a heterogeneously hyper intense schwannoma (asterisk) at the carotid bifurcation splaying the internal (short arrow) and external (long arrow) carotid arteries. A second schwannoma is seen widening the right C2-C3 neural foramen (thin arrow) with mild mass effect upon the spinal cord. (**H**) Coronal T1-weighted image with contrast again shows the lesion at the C2-C3 neural foramen which appears enhancing with slight heterogeneity (thin arrow). A third schwannoma from a 56 year-old female with schwannomas (II-2) is demonstrated subjacent to the right sternocleidomastoid muscle (thick arrow), showing peripheral enhancement with central cystic degeneration. (**I**) Photograph of the schwanomma in the left foot of II-2. (**J**) Photograph of the schwannoma in the right knee of II-2.

Supplementary Figure 2. Histology of the tumors in the index family

Multinodular goiters (MNGs)

Schwannomas

Choroid plexus papilloma (CPP)
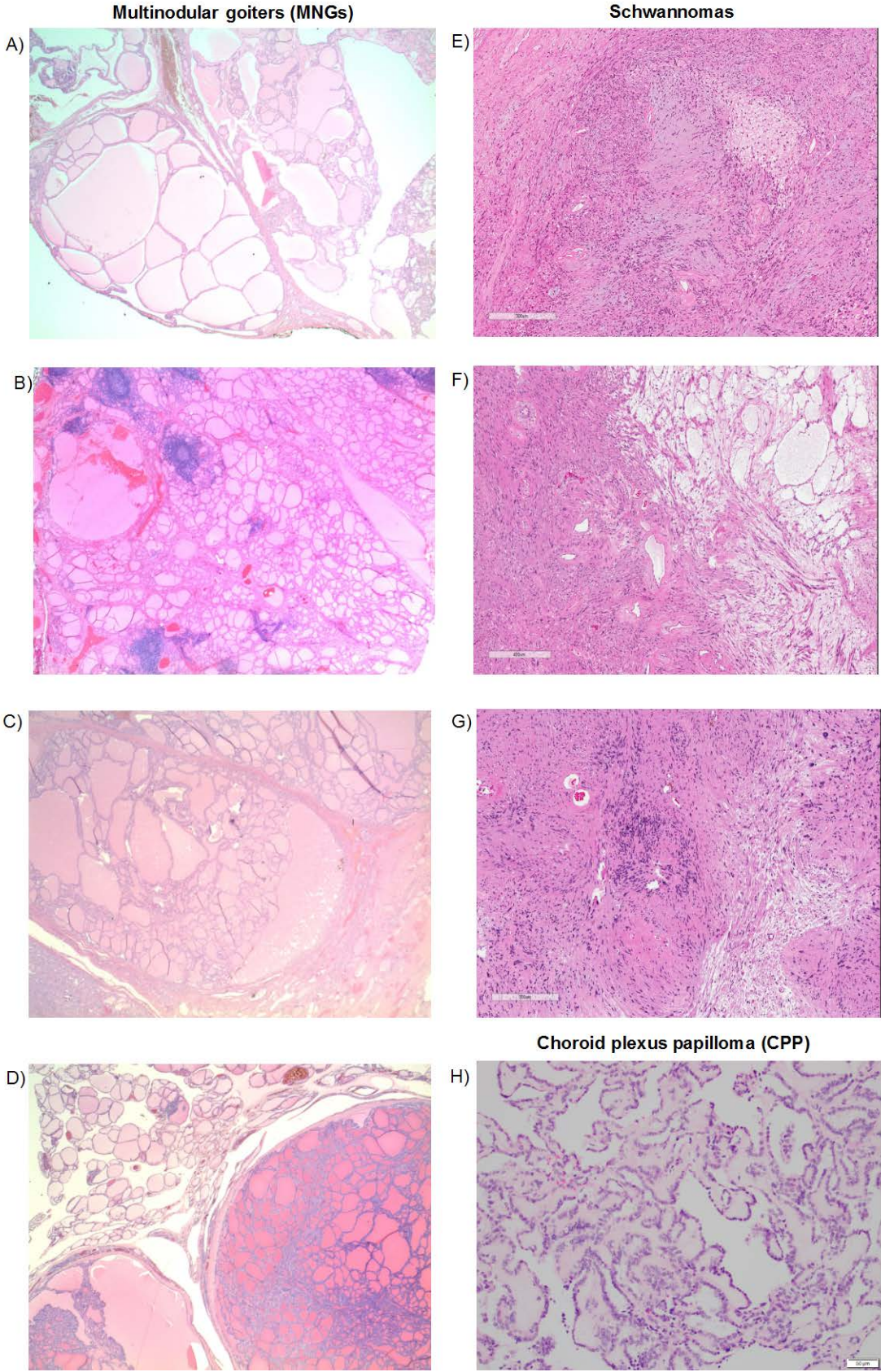
Supplementary Figure 2. (A-D) Representative images of H&E stained multinodular goitre (MNG) of the proband (II-1), individuals III-1, III-2 and III-3, respectively. Original magnification, 20X. **(E-G)** Representative images of H&E stained schwannomas of persons II-2, III-2 and I-1, respectively. Scale bars: 400 μm, 300 μm, 300 μm. **(H)** Representative image of H&E stained choroid plexus papilloma (CPP) of individual III-1. Scale bar: 50 μm.

Supplementary Figure 3. Conservation of c.1552G across species
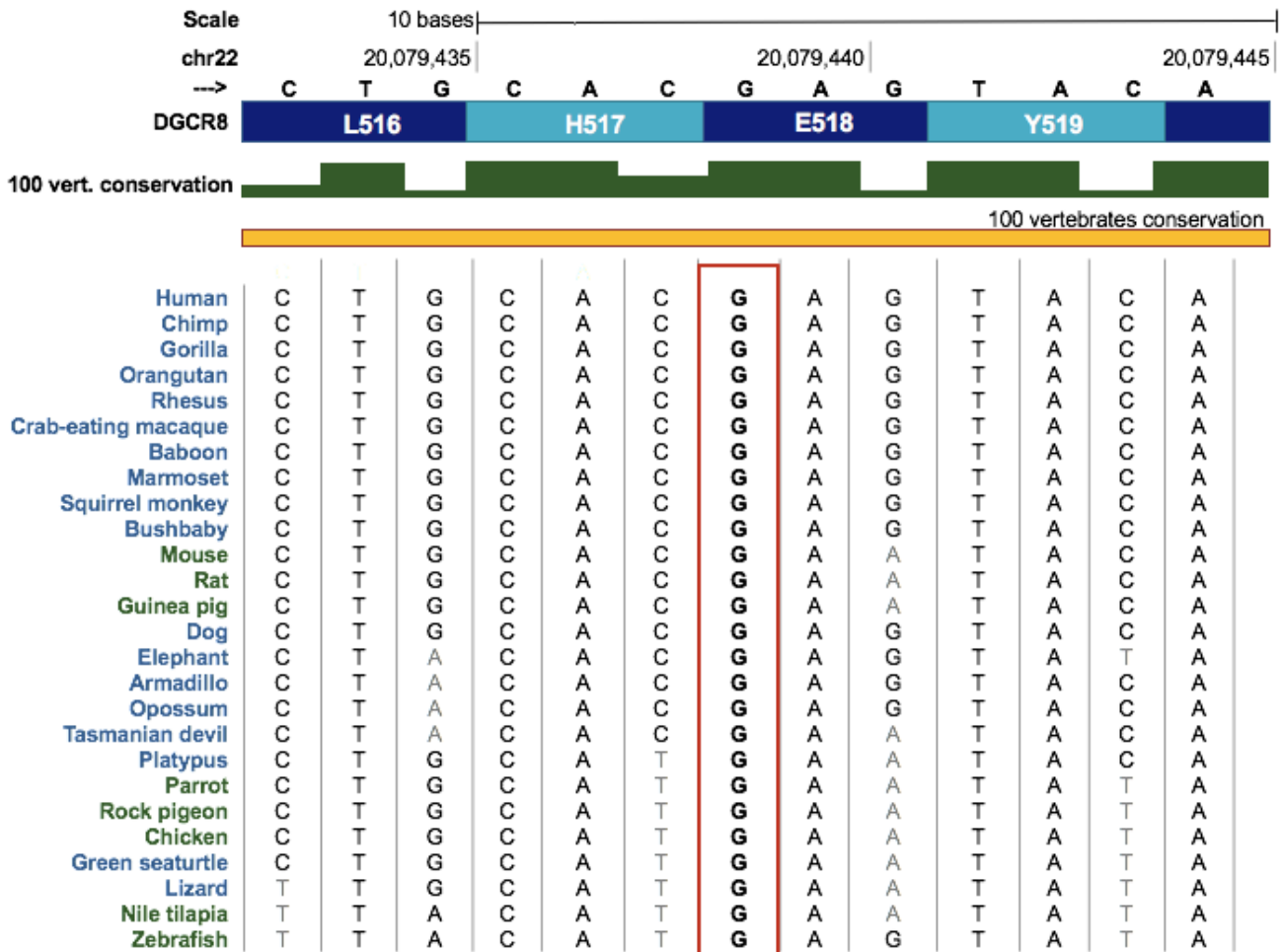
Supplementary Figure 3. Nucleotide position c.1552G (corresponding to the first base pair of codon 518, highlighted in a red box) is highly conserved among species of vertebrates. Data was obtained through the UCSC genome browser (www.genome.ucsc.edu) based on (GRCh37/hg19) assembly.

Supplementary Figure 4. Analysis of expression of *DGCR8* mutated allele c.1552G>A;p.E518K

Germline cDNA from III-3

Germline cDNA from a control

Supplementary Figure 4. The presence of the wild type base G and the mutated base A at the position of the asterisk demonstrates that the variant c.1552G>A;p.E518K is expressed together with the wild type allele.

Supplementary Figure 5. Genome-wide Allelic Imbalance (LOH) analyses in Schwannomas, Choroid Plexus Papilloma, Papillary Thyroid Cancer and Wilms Tumors bearing *DGCR8*-c.1552G>A;p.E518K
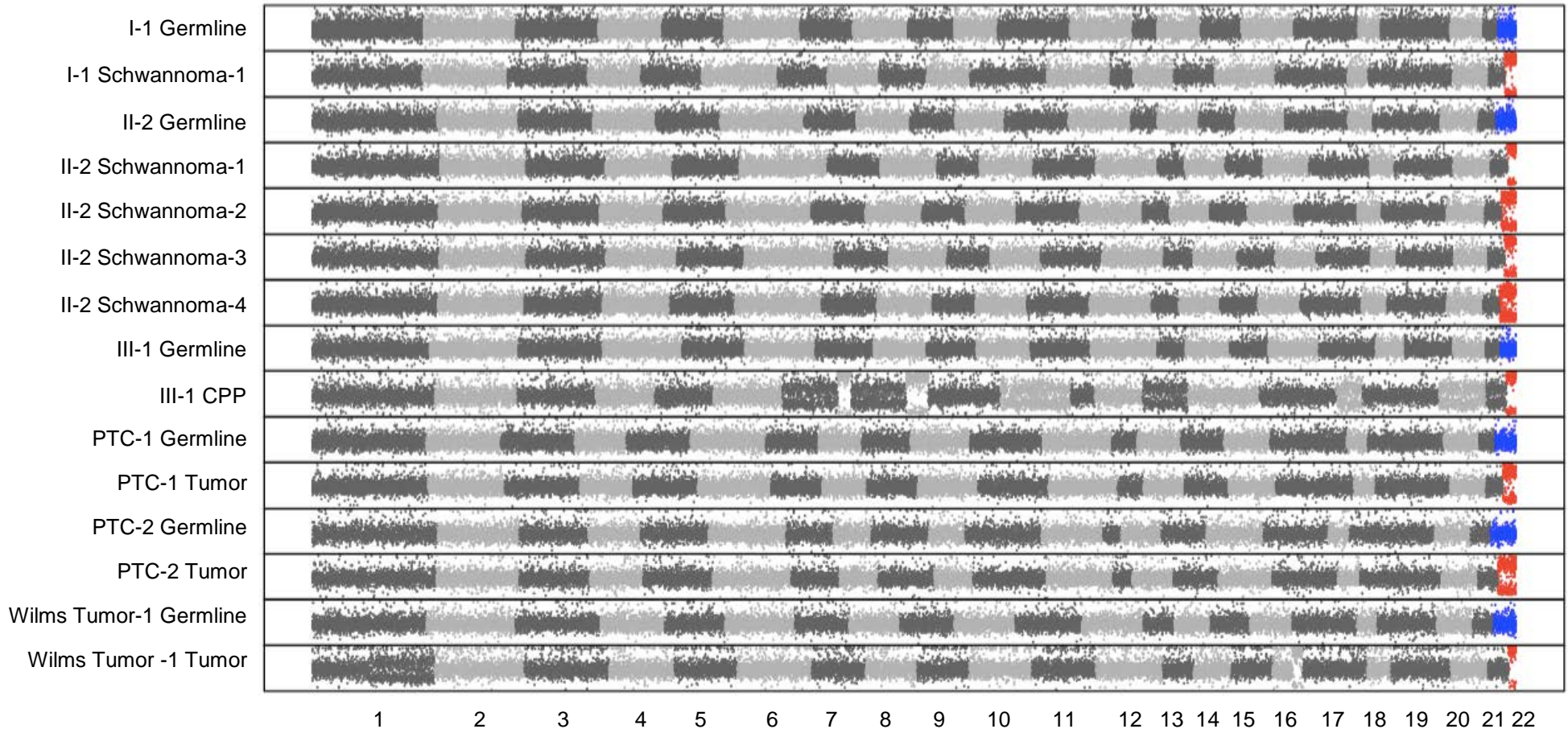
Supplementary Figure 5. Germline and tumor genome-wide allelic imbalance (LOH) analysis in a set of 8 DGCR8-E518K mutated tumors and their corresponding paired germline samples. Genome-wide recurrent plot of Allelic Imbalance (AI) are generated by ExomeAI(34) from samples subjected to WES in the present study (tumors from the family index) or from publicly available data (WES from Follicular variant PTC-1 and 2 and WGS from Wilms Tumor-1). WES confirmed a loss of the entire Chr22 in all tumors analyzed. The x-axis lists chromosomes according to their number. Each row is one sample. *DGCR8* is located on chromosome 22. Blue color on Chr22 means no aberration (germline samples); red color, LOH (tumor samples).

Supplementary Figure 6. Genome-wide copy number analysis using SNP-arrays (OncoScans) in MNGs of individuals II-2, III-1, III-2, III-3 and in the two PTC samples with the c.1552G>A;p.E518K mutation in *DGCR8*
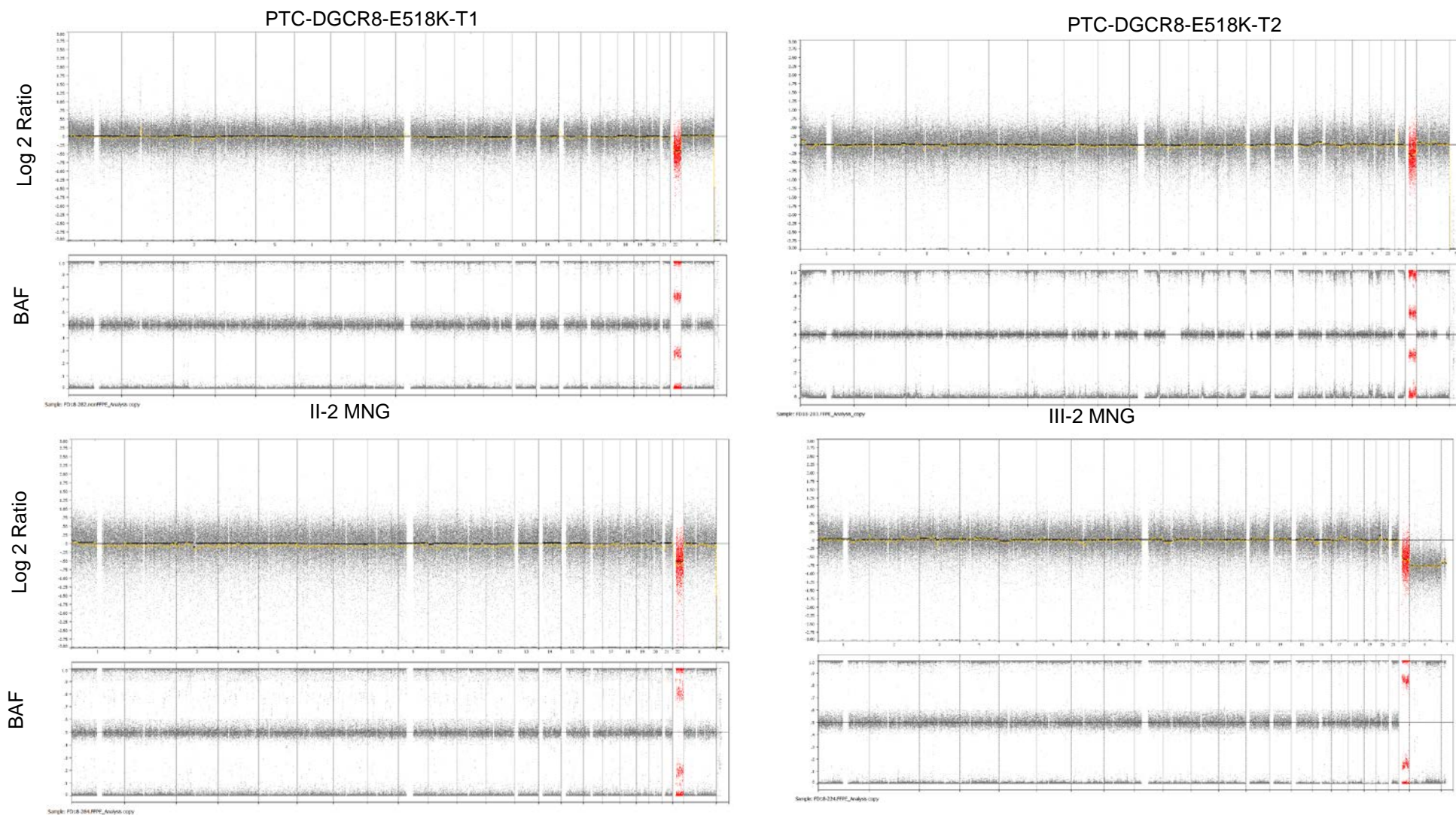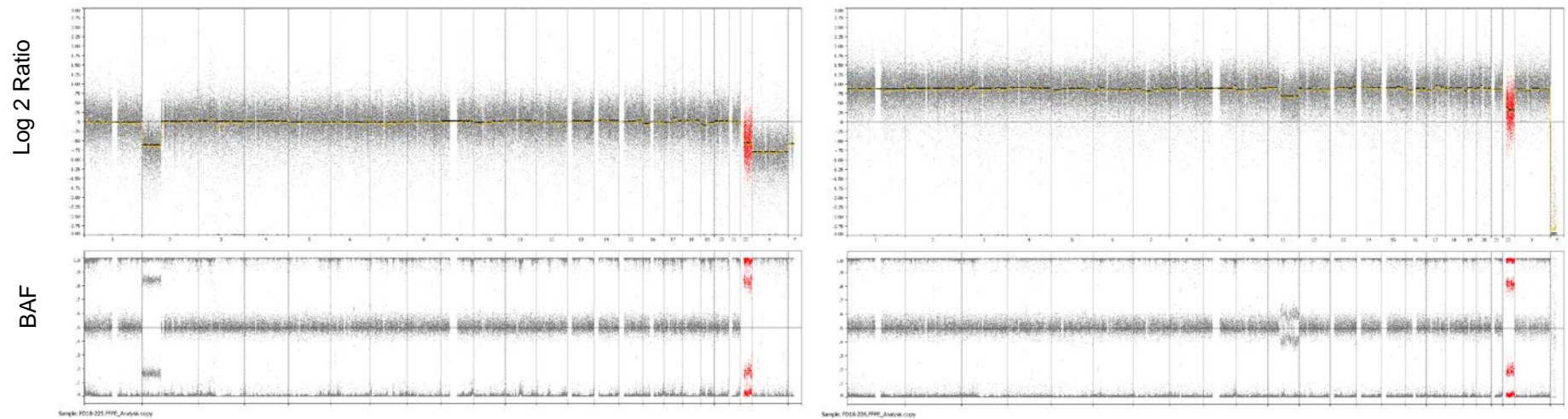
Supplementary Figure 6. Genome-wide plot of copy number alterations (CNA) in MNGs of individuals II-1, II-2, III-1, III-2, III-3 and in the two PTC (follicular variant) samples with the E518K mutation in *DGCR8*. In the genome wide plots of imbalances the X-axis represents the genome from chromosome 1p to Y. Imbalance (upper panels) and B-allele frequency (BAF, lower panels) plots. In the imbalance plots, the Y axis gives the log2 ratio correlating to the intensity ratio of each probe of the analyzed sample in comparison to a reference. Dots represent balanced areas in the tumor which are centered around 0. In the BAF plots, values of 0 and 1 indicate (germline) homozygosity and values of around 0.5 heterozygosity (i.e. an equal number of two different alleles). In all samples, the BAF of non-homozygous calls is skewed away considerably from the 0.5 value indicating allelic imbalance at Chr22 (highlighted in red). As can be seen from the BAF plots, the only alteration common in all MNG and PTC samples was the allelic imbalance at the Chr22 in line with all samples showing an homozygous genotype at the *DGCR8* locus. These can be due to different mechanisms like deletion of (a) Chr22 allele(s) from overall ploidy, or as in III-3 a complex gain leading to a 4n genome and a loss of the Chr22 allele from the mother (resulting in a copy-neutral LOH). These results are also in concordance with the genome alterations shown in the schwannomas and CPP from the family members and DGCR8-E518K Wilms Tumor, LOH being the common event among all samples. The PTC samples were also analyzed by WES and showed allelic imbalance in Chr22 confirming a loss of Chr22. The loss of Chr22 resulting in LOH in the MNGs was also confirm by the presence of allelic imbalances in the Haplexplex[HS] data and Sanger sequencing both showing an overall absence of the wild type allele.

Supplementary Figure 7. Functional in silico characterization of the c.1552G>A, p.E518K variant in *DGCR8*
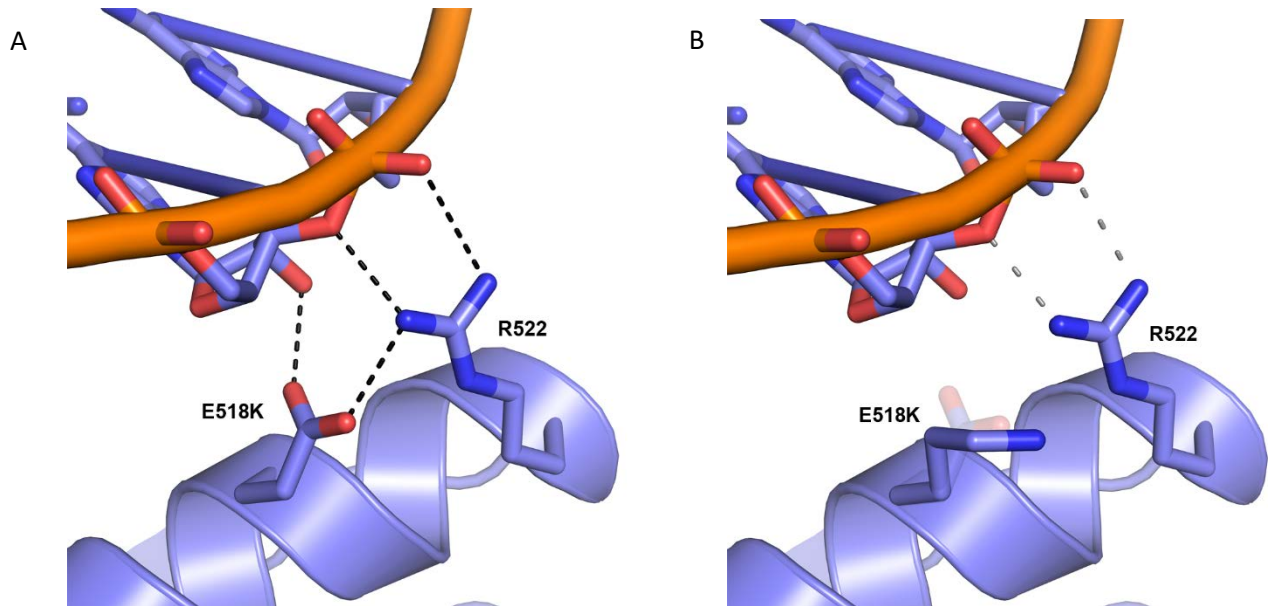
Supplementary Figure 7. A) Cartoon diagram of the structure of wild type DGCR8 bound to double stranded RNA showing the environment around residue 518. Residue E518 is located in the double stranded ribosome binding domain and makes a hydrogen bond interaction with the ribose of a RNA nucleotide. E518 is also forming a hydrogen bond with R522, a residue involved in interactions with the phosphate backbone of RNA. **B)** Cartoon diagram illustrating the impact of the E518K mutation. For reference the wild type E518 is also depicted in semi-transparent stick representation. The mutation of E518 to lysine, results in the abolishment of a hydrogen bond between DGCR8 and the RNA. Additionally, the two hydrogen bonds between R522 and the RNA phosphate backbone would likely be weakened, as the arginine is no longer anchored by residue 518. Finally, the E518K mutant would create an unfavorable charge environment, with two positively charged residues, lysine and arginine, now in close proximity. For these reasons, it is expected that this mutation will reduce the affinity of DGCR8 for double stranded RNA.

Supplementary Figure 8. Consensus clustering of miRNA expression analysis in the Schwannoma and Wilms Tumor datasets

A **Consensus CDF**

B **Consensus Matrix k = 2**
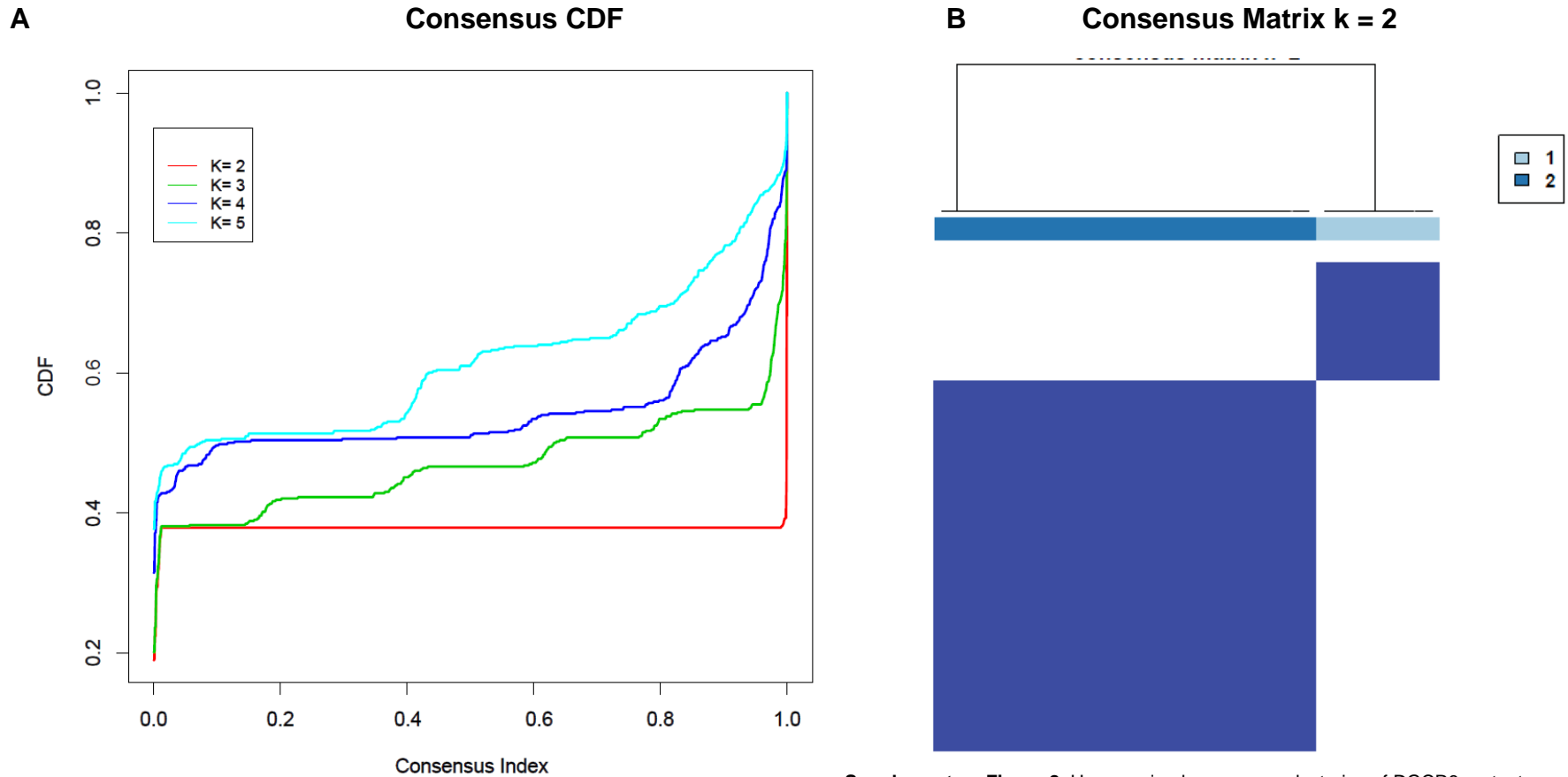
Supplementary Figure 8. Unsupervised consensus clustering of DGCR8-mutant samples and their wild type counterparts (n sample = 33) using normalized miRNA expression values. The clustering was evaluated for 2 up to 5 clusters (k = 2 to 5), with 1000 repetitions with subsampling 80% of all miRNAs at each repetition.
A) Consensus distributions for each k using empirical Cumulative Distribution Function (CDF) plot for each K from 2 to 5. As the CDF plot clearly shows, the 2-cluster solution performs best with lowest Proportion of Ambiguous Clustering. **B)** Consensus membership matrix for 2-cluster solution (k = 2).

Supplementary Figure 9. Multidimensional scaling visualization of miRNA expression in *DGCR8*-c.1552G>A;p.E518K mutated tumors and their wild type counterparts
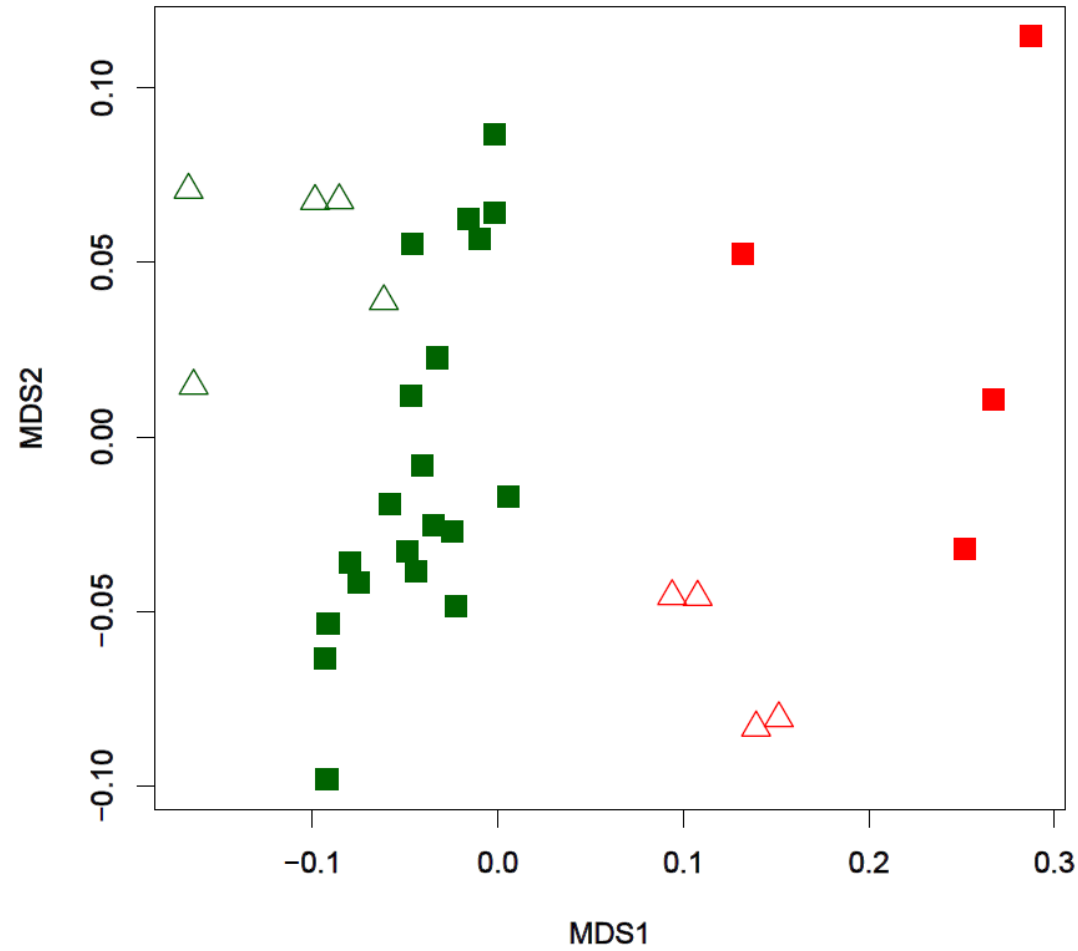
Supplementary Figure 9. Multi-Dimensional Scaling (MDS) plot of miRNA expression (the same data as Figure 3A). The primary MDS axis (MDS1) can separate DGCR8-mutant Wilms tumors and DGCR8-mutant Schwannomas (MDS1 < 0.01) from their wild type counterparts (MDS1 > 0.09). Rectangles: Wilms tumors; Triangles: Schwannomas; Red: DGCR8-mutant; Green: DGCR8-wild type

Supplementary Figure 10. Comparison among the differential expression analysis in the Schwannoma and Wilms Tumor datasets

A

B
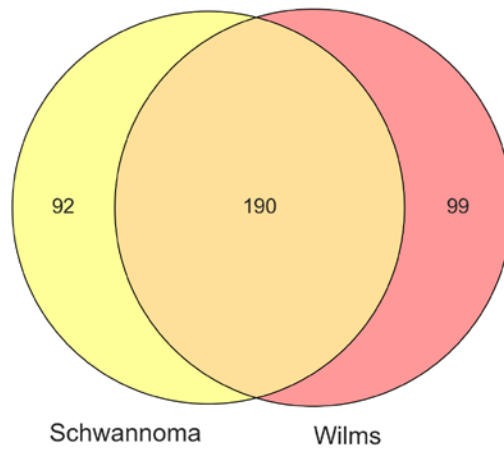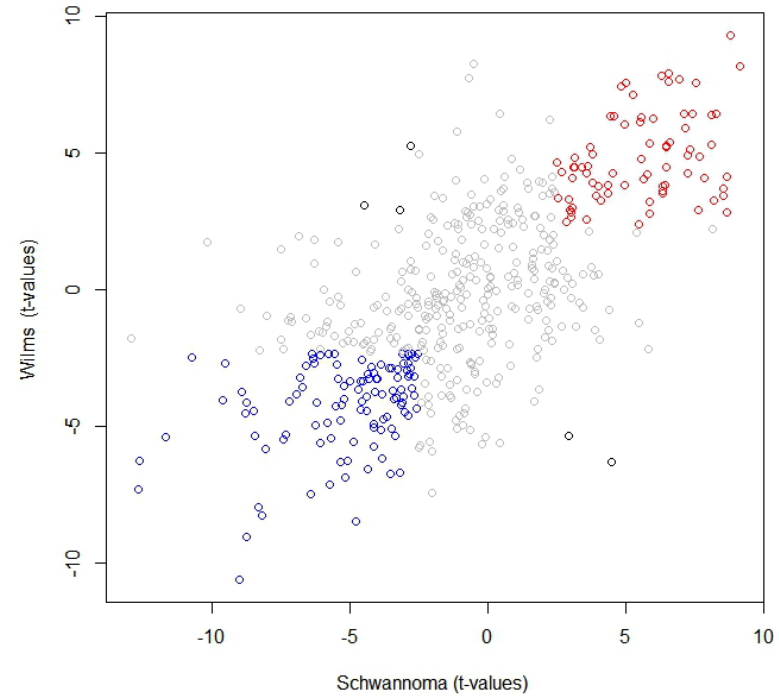
Supplementary Figure 10. miRNA differential expression analysis (DGCR8 mutated vs DGCR8 wild type tumors) was performed separately for each dataset. **A)** The Venn diagram shows that about two-thirds (n = 190) of the differentially expressed miRNA (FDR <0.01) in each dataset are shared among the two. **B)** The scatter plot shows that the differentially expressed miRNA are regulated in the same direction for both datasets (red: overexpressed in DGCR8-mutated tumors, blue: under expressed).

Supplementary Figure 11. Pre-miRNA clustering of *DGCR8*-c.1552G>A;p.E518K mutated tumors and their wild type counterparts
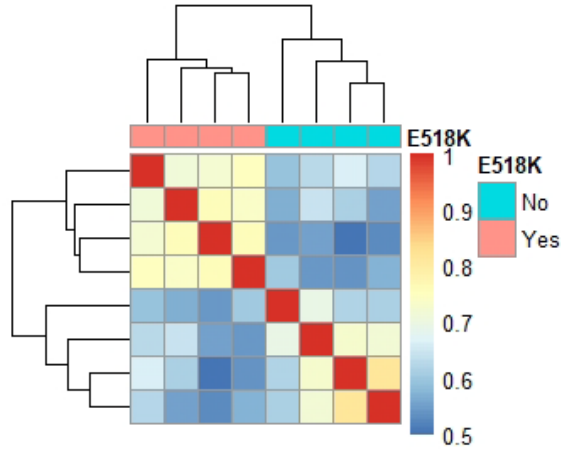
Supplementary Figure 11. Unsupervised hierarchical pre-miRNA expression clustering of 4 DGCR8-E518K mutated schwannomas from II-2, and 4 DGCR8 wild type schwannomas from controls. DGCR8-E518K mutated and DGCR8 wild type samples separate from each other based on their pre-miRNA profiles as expected. The total number of pre-miRNA identified was n = 251, all 251 were used in the clustering.

Supplementary Figure 12. Pre-miRNA Differential Expressed (DE) analysis of tumors with or without *DGCR8* mutation
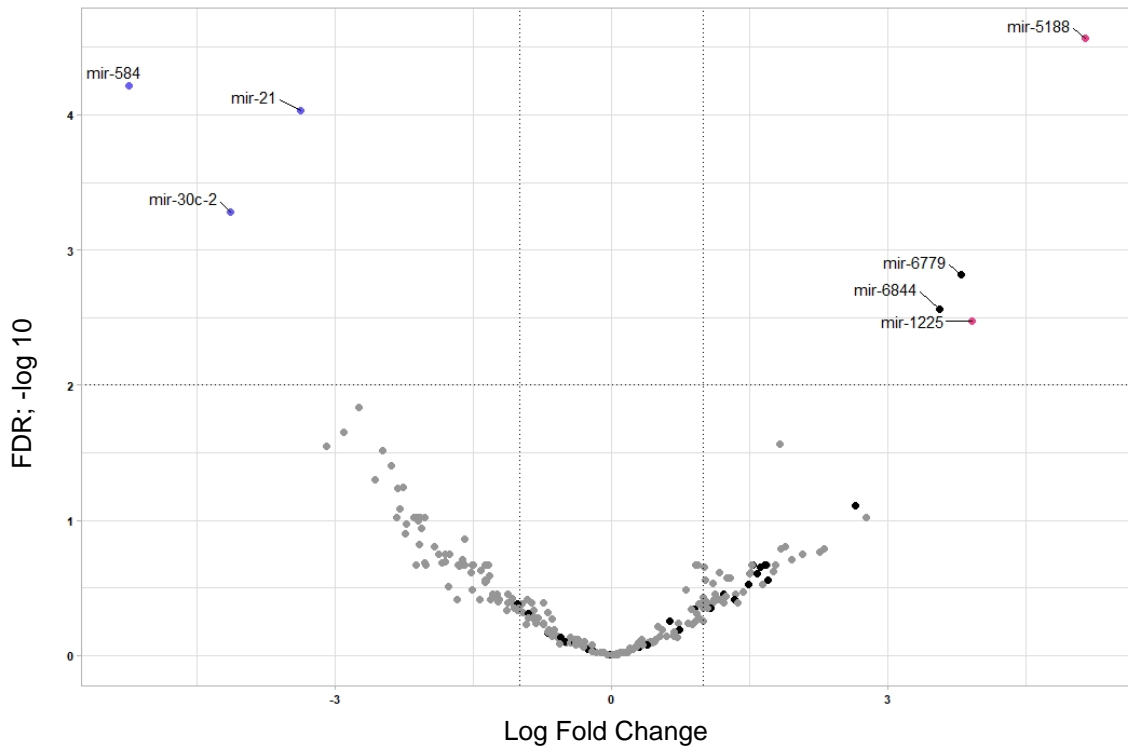
Supplementary Figure 12. The volcano plot shows the results of DE pre-miRNA expression analysis between schwannoma cases with (n = 4) and without *DGCR8* mutation (n = 4). Upregulated and downregulated pre-miRNAs in DGCR8 mutated cases are shown in red and blue, respectively. Black dots represent the non-canonical intronic miRNAs, mirtrons. Log Fold Change is plotted on the x-axis and adjusted p-value (FDR; -log10 scale) on the y-axis. Horizontal and vertical lines indicate threshold of significance (FDR <0.01; absolute fold change >2). One of the most significantly under expressed pre-miRNAs, miR-30-c-2, is the precursor for the most significant underexpressed mature miRNA. Overrepresentation of mirtrons was validated using mature miRNAs in 2 different datasets (Figure 4B, Figure 4D).

Supplementary Figure 13. In vitro cleavage with pri-miR-223
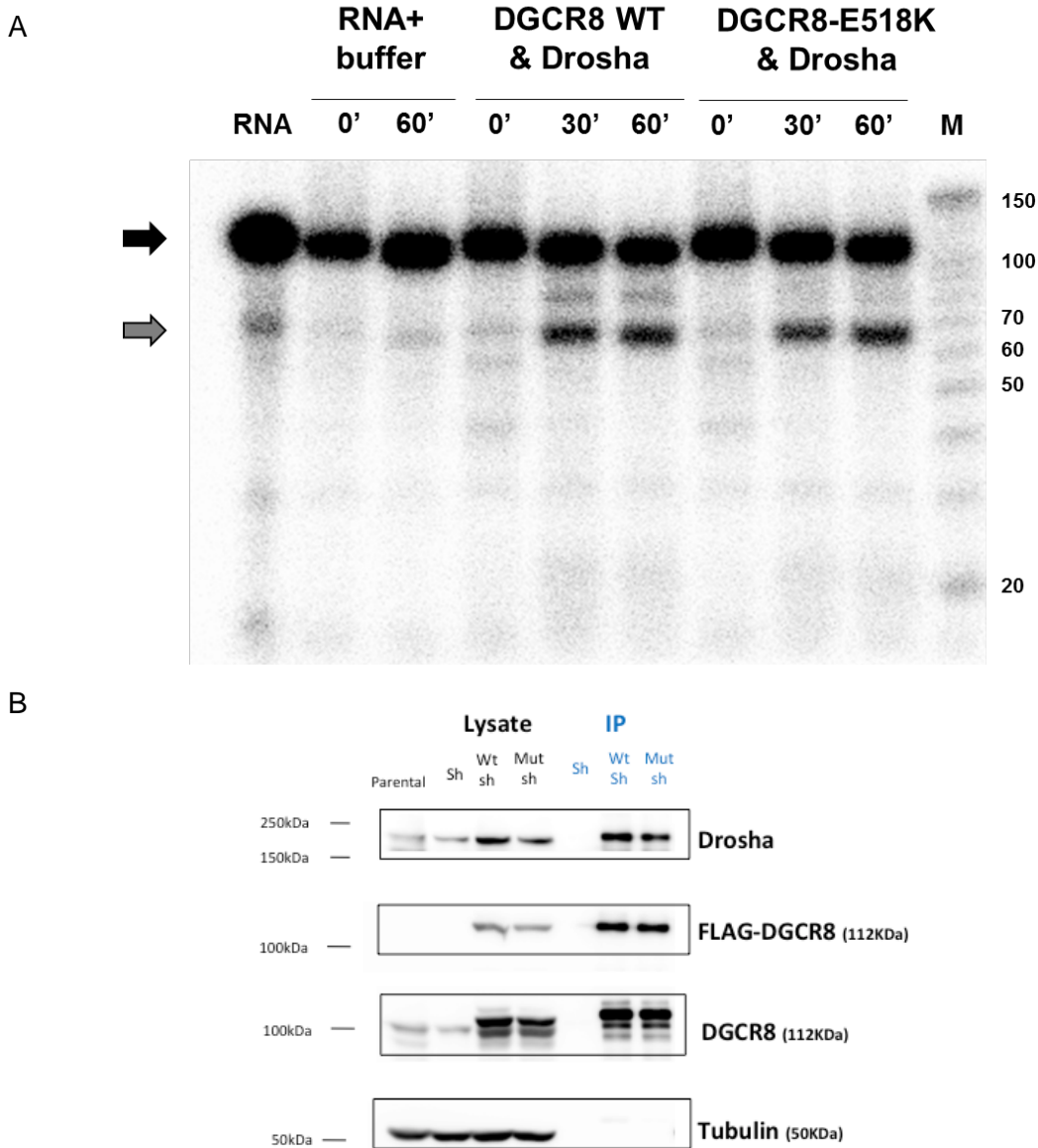
Supplementary Figure 13. A) In vitro cleavage assay for DGCR8-Drosha wild type (WT) and DGCR8-E518K-Drosha (Mutant) using the pri-miR-223 hairpin. Given that miR-223 was not differentially expressed among DGCR8 mutated tumors vs DGCR8 wild type counterparts, pri-miR-223 was selected as a positive control for the cleavage experiment. The expected pattern of cleavage is shown in DGCR8 WT-Drosha, with cleavage of the pri-miR-223 hairpin occurring over 60 minutes, leading to a diminution of the intensity of the pri-miR-223 band at 100 nucleotides and production of pre-miR-223 over the same time. The image is representative of three independent replicate experiments. In each experiment, three conditions were tested, and freshly immunoprecipitated

proteins were used in each case. DGCR8-E518K-Drosha (Mutant) showed production of pre-miR-223 over the same time, almost with the same intensity as with DGCR8-Drosha wild type. A radiolabeled RNA molecular weight marker was loaded in every assay, shown as "M". "RNA" means only the pri-miR-223 was added. The experiment was done in triplicate. **B)** Blots showing DGCR8 expression in the lysates and immunoprecipitated FLAG-DGCR8. Tubulin was included as loading control. Immunoprecipitated proteins were used for the in vitro cleavage assays with primaries miR-30c-2 and miR-223. Primary miR-223 was used as a control.

Supplementary Figure 14. miRNA Differential Expressed (DE) analysis of tumors with or without *DICER1* mutation

Log Fold Change
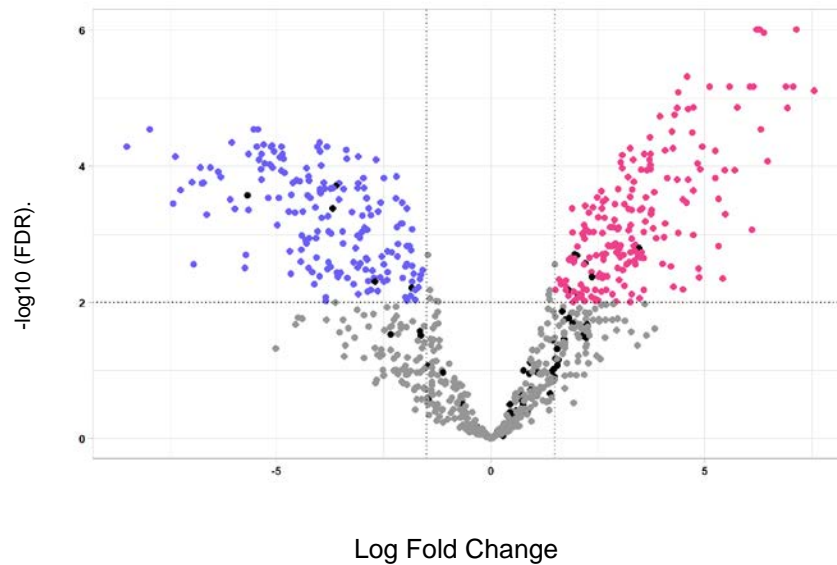
Supplementary Figure 14. The volcano plot shows the results of DE miRNA expression analysis between pituitary blastoma cases with *DICER1* mutations (n = 3) versus normal pituitary *DICER1* wild type (n = 7; 4 adult and 3 fetal samples). Overexpressed and under expressed miRNAs in DICER1 mutated cases are shown in red and blue, respectively. Black dots represent the non-canonical intronic miRNAs, mirtrons that appear in both in contrast to DGCR8 mutated schwannomas and Wilms Tumors. Log Fold Change is plotted on the x-axis and adjusted p-value (FDR; -log10 scale) on the y-axis. Horizontal and vertical lines indicate threshold of significance (FDR <0.01) absolute fold change (>2). Axes: X: Log Fold Change; Y: -log10 (FDR).

Supplementary Figure 15. Gene Set Enrichment Analysis of DGCR8 mutated vs. wild type Schwannomas
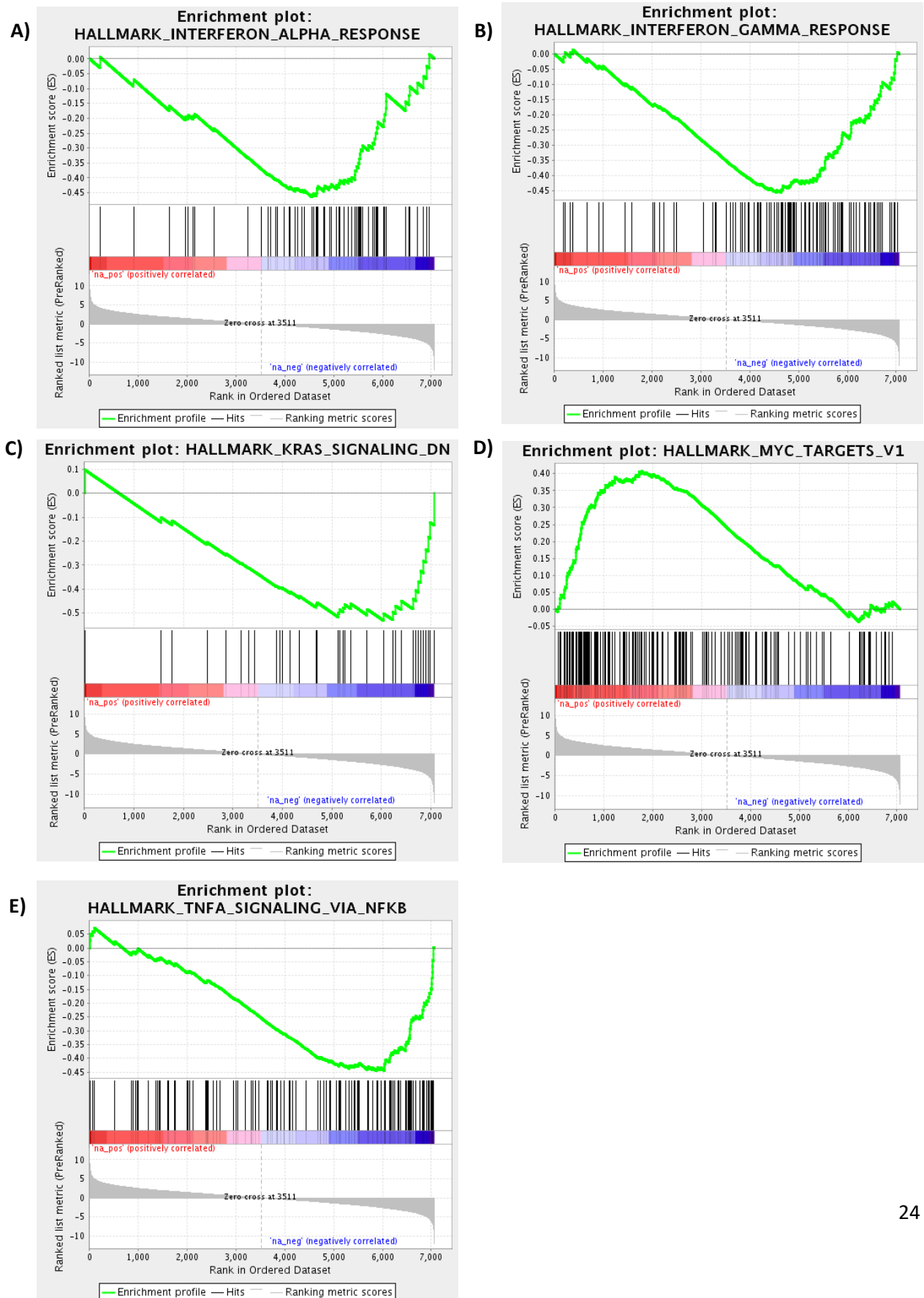
Supplementary Figure 15. Gene Set Enrichment Analysis(24), based on comparison between DGCR8-mutated and wild type schwannomas, using 50 Hallmark Gene Sets(25). Enrichment plots for the 5 significantly enriched gene sets (out of 50) with FDR less than 0.01 (NES > 1.9 or NES < -1.9) are shown (See also Supplemenetary Table 13). **A)** HALLMARK_INTERFERON_ALPHA_RESPONSE; **B)** HALLMARK_INTERFERON_GAMMA_RESPONSE; **C)** HALLMARK_KRAS_SIGNALING_DN (Genes down-regulated by KRAS activation(7)); **D)** HALLMARK_MYC_TARGETS_V1; **E)** HALLMARK_TNFA_SIGNALING_VIA_NFKB

Supplementary Figure 16. Chromosomal location of *DGCR8, LZTR1, SMARCB1* and *NF2* along Chr22
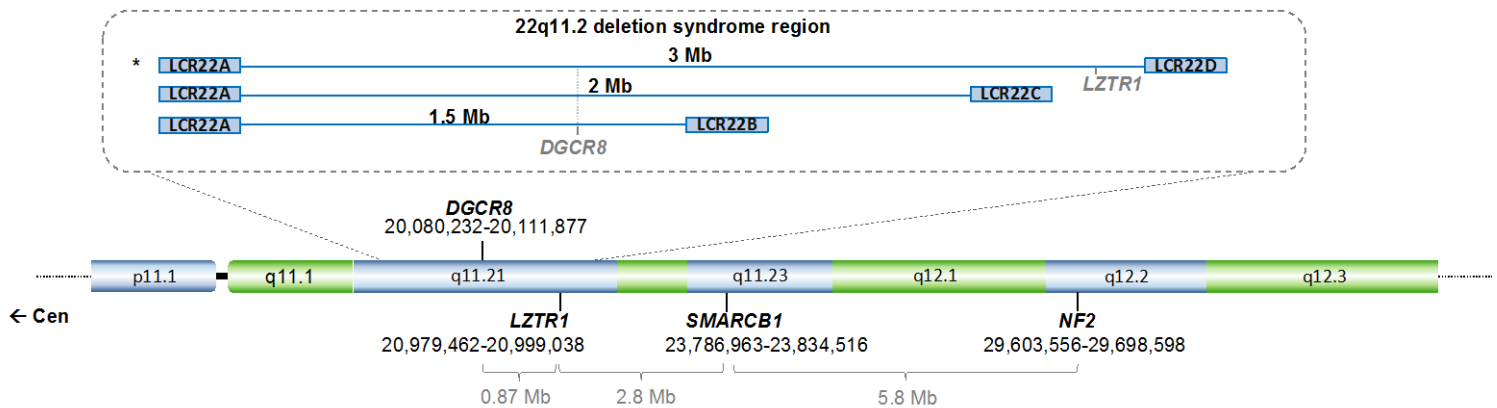
Supplementary Figure 16. Chromosomal locations and distances among genes [shown in megabases (Mb) with horizontal brackets] are based on (GRCh37/hg19) assembly. Data was obtained from Ensembl genome browser (https://grch37.ensembl.org/index.html).

Supplementary Figure 17. Genotype-phenotype association of previously described mutations in the literature and public databases

	LOCATION	TUMOR TYPE
	Skin	Melanoma
	Skin	Squamous Cell Carcinoma
	Skin	Basal Cell Carcinoma
	Lung	Non Small Cell Lung Cancer
	Lung	Squamous Cell Carcinoma
	Lung	Adenocarcinoma
	Stomach	Adenocarcinoma
	Esophagus	Squamous Cell Carcinoma
	Esophagus	Adenocarcinoma
	Breast	Lobular Carcinoma
	Head and Neck	Squamous Cell Carcinoma
	Colon	Adenocarcinoma
	Kidney	Wilms Tumor
	Kidney	Clear Cell Renal Carcinoma
	Kidney	Renal Cell Carcinoma
	Cervix	Squamous Cell Carcinoma
	Uterus	Endometrioid Carcinoma
	Uterus	Serous Carcinoma
	Liver	Hepatocellular Carcinoma
	Liver	Hepatocellular Adenoma
	Thyroid	Thyroid Carcinoma
	Thyroid	Multinodular Goiter
	NS	Schwannoma
	Brain	Choroid Plexus Tumors
	Brain	Glioma
	Bladder	Urothelial Carcinoma
	Biliary Tract	Biliary Tract Carcinoma
	Pancreas	Adenocarcinoma
	Prostate	Adenocarcinoma
		Other

Missense Variants
Nonsense Variants
Splice Variants
Frameshift Variants
Start-lost Variants

SOMATIC

NLS	WW	Rhed		dsRBD1		dsRBD2	Drosha-binding

1   275 300 334   498 510   578 618   686   773
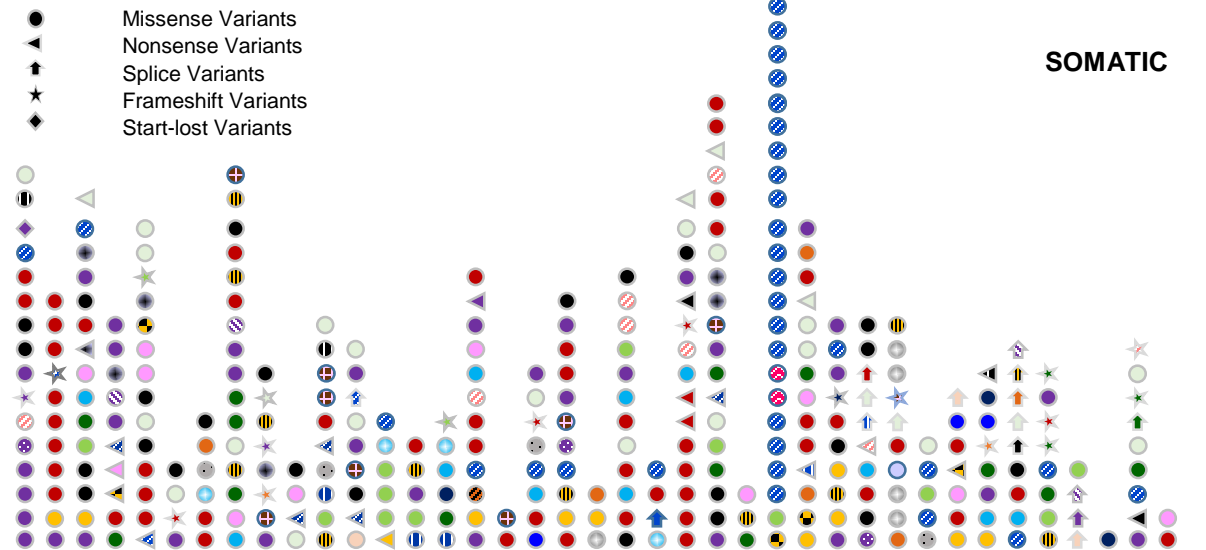
FAMILY 1
1

*

GERMLINE   26

Supplementary Figure 17. Germline mutations are shown at the bottom of the protein sequence, somatic mutations at the top. If no germline DNA was available, variants identified in tumors were plotted as somatic by default. The shapes refer to the type of mutation while color code refers to associated pathology as noted in the color key. *Note,* Wilms Tumors cluster exclusively within the p.E518K hotspot.

Asterix: The germline variant K588R has been listed in the literature. The general allele frequency is 0.6% in ExAC(26), which is greater than the pathogenic allele-frequency threshold ≤0.1%. Apart from the two Wilms tumors taken from the literature containing variant p.K588R, we also identified p.K588R in 7 out of 181 tumors sequenced. Two out of the 7 are from the same patient (2 schwannomas) and was plotted once as germline. The six remaining samples were plotted as somatic (1 CPT and 5 schwannomas). However, our NanoString analysis confirmed a miRNA profile for the p.K588R similar to a wild type sample. Although we have kept it in the plot, all this data indicates that this variant is likely a benign polymorphism. Domains of DGCR8 are color coded. The double strand RNA binding domain 1 (dsRBD1) and double strand RNA binding domain 2 (dsRBD2) are both shown in green. Drosha binding domain as well as the RNA-binding heme domain (Rhed) are shown in yellow. Red shows the dimerization domain (WW) and in blue is the nuclear localization signal (NLS).

Data was taken from ICGC dataportal (https://dcc.icgc.org; last accessed 03/2018), **TumorPortal** (http://www.tumorportal.org; last accessed 03/2018), **cBioportal** (http://www.cbioportal.org; last accessed on 25/06/2018), **Decipher**, **COSMIC** (https://cancer.sanger.ac.uk/cosmic; last accessed 5/07/2018).

We removed variants in the following categories:

(A) MUTATION TYPE: Intronic, UTRs, synonymous, upstream, downstream; (B) FREQUENCIES: gNOMAD ≥0.001, 1KMAF ≥0.001, EXAC ≥0.001, rs ≥0.001; (C) PREDICTORS: 3 out of 4 were benign (PPH2,SIFT, CONDEL, MutTaster or MutAssessor) and CADD ≤20; (D) Duplicates and Triplicates of samples.

Supplementary Tables

Supplementary Table 1. Germline variants of index family (WES) (family segregation)

Gene		*COL6A2*	*DGCR8*
Gene info		NM_001849: ex10:c.G988A;p.D330N	NM_022720: ex6:c.G1552A;E518K
Individual	**II-1**	(het) –VAF=0.492	(het) - VAF=0.409
	I-1	(het) - VAF=0.425	(het) - VAF=0.511
	II-2	(het) - VAF=0.605	(het) - VAF=0.468
	III-1	(het) - VAF=0.544	(het) - VAF=0.523
	III-2	(het) - VAF=0.513	(het) - VAF=0.349
	III-3	(het) - VAF=0.452	(het) - VAF=0.478
	II-4	-	-
	II-3	-	-
	III-5	-	-
rsID138		rs139399166	-
1000G_MAF*		0.00019968	0
EVS_MAF*		0.000384	0
ExacNoTCGA_MAF*		3.00E-04	-
gnomad_MAF*		0.0002	-
Homozygotes_EXAC		0.000304	-
COSMIC_ID		COSM1201959	COSM3371859
SIFT**		0.11, 0.89, T	0, 1.00, D
Polyphen2**		0.997,D	0.999,D
MutationTaster**		1,1.0,D	1,1.0,D
Revel**		0.456	0.819
MCAP**		0.2347232	0.27728257
CADD_phred**		33	35

* Minor allele frequency (MAF) in the 1000 Genome project (http://www.1000genomes.org/home), EVS (Exome Variant Server; http://evs.gs.washington.edy/EVS/), Non-TCGA ExAC (The Exome Aggregation Consortium; http://exac.broadinstitute.org/), gnomAD (http://gnomad.broadinstitute.org/), KAVIAR (http://db.systemsbiology.net/kaviar/) and Greater Middle East (http://igm.ucsd.edu/gme/) databases. VAF= Variant allele frequency
** Functional impact prediction results of 6 bioinformatics algorithms. The Revel score changes between 0 to 1 and more damaging variants have higher scores. CADD score ≥20 indicates deleterious variants.

Supplementary Table 2. Coverage data for the WES experiment in the germline of 9 members of the family

Sample_id	Mean	%CCDS bases ≥ 5x coverage	%CCDS bases ≥ 10x coverage	%CCDS bases ≥ 20x coverage	%CCDS bases ≥ 50x coverage
II-1	134	98.5	98.1	97.4	92.5
I-1	92	98.1	97.2	94.7	79.2
II-2	167	98.3	98.0	97.4	93.4
III-3	238	98.4	98.0	97.2	94.0
II-4	90	98.3	97.8	95.9	73.1
III-4	122	98.3	97.8	96.6	87.5
III-2	137	98.6	98.3	97.4	90.7
III-1	131	98.6	98.2	97.2	89.7
II-3	136	98.6	98.2	97.6	91.3

Supplementary Table 3. Loss of heterozygosity (LOH) summary in tumors of the index family

PEDIGREE	I-1	II-1			II-2				III-1					III-2				III-3				
Lesion	Schw	MNG			Schw				MNG	CPP	MNG			Schw	MNG			MNG			Schw	
	1	1	2	3	1	2	3	4	1	1	1	2	3	1	1	2	3	1	2	3	1	2
E518K-LOH	+	+	-	+	+	+	+	+	+	+	+	+	+	+	+	+	+	+	+	+	+	+
DGCR8 LOH/ Chr22 loss	Chr22-Loss	NA	NA	LOH	Chr22-Loss	Chr22-Loss	Chr22-Loss	Chr22-Loss	Chr22-Loss	Chr22-Loss	Chr22-Loss	LOH	LOH	LOH	Chr22-Loss	LOH	LOH	CN-LOH	LOH	LOH	LOH	LOH

The MNGs tissue from II-1, III-1, III-2 and III-3 were studied by a Haloplex^HS. DNA was extracted from 3 different nodules. For each individual, the presence of LOH at the variant c.1552G>A;p.E518K locus in every nodule was validated by Sanger sequencing. + corresponds to presence of LOH at the E518K locus. All samples tested showed LOH at the E518K locus except for 1 nodule out of three in individual II-1. No variant in other miRNA processing genes (*DICER1, DROSHA, DIS3L2, XPO5, AGO2* and *TARPB2*) was found. Loss of heterozygosity extended to the entire *DGCR8* locus was confirmed by HHS results (as explained in the methods section; Threshold = 0.25. Cutoff = 66%). For nodule #1 in individual II-1, we could not calculate the length of LOH because of low coverage. NA: Not done. In parallel, the genome wide copy number status of MNG nodules #1 of II-2, III-1, III-2 and III-3 were studied by OncoScans. A loss of Chr22 was confirmed in II-2, III-1 and III-3 demonstrating that the LOH seen in the Haloplex and Sanger sequencing results from the loss of the wild type copy of Chr22, indicated in the table as Chr22-loss. The nodule #1 of III-1 showed a tetraploid genome except for Chr22 (2n) and presence of LOH demonstrating a copy neutral LOH (indicated as CN-LOH). An allelic imbalance showing LOH and loss of Chr22 was also seen in all schwannomas tested by WES (from individuals I-1 and II-2) and the CPP from III-1. The schwannomas from individuals III-2 and III-3 were tested by Sanger sequencing which confirmed LOH at the E518K locus. The whole *NF2* gene was tested in the schwannomas from III-2 and III-3 by Sanger sequencing. The schwannoma from III-2 had a truncating variant in *NF2*, c.112G>T;p.E38* and the two schwannomas from individual III-3 each had one truncating variant in *NF2*, c.592C>T;p.R198* and c.199_226delACAATCAAGGACACAGTGGCCTGGCTCA;p.T67Kfs*47, respectively.

Supplementary Table 4. Somatic mutations found by WES in 5 schwannomas from index family individuals (4 schwannomas from individual II-2, 1 schwannoma from individual I-1)

Gene	Gene Info	II-2 schw1 (VAF)	II-2 schw2 (VAF)	II-2 schw3 (VAF)	II-2 schw4 (VAF)	I-1 Schw (VAF)	rsID138	ExacNo TCGA_ MAF*	gnomad MAF*	COSMIC _ID	SIFT**	Polyphen 2**	Mutation Taster**	Revel **	MCAP**	CADD _phred **
METTL11 B	NM_001136107: ex2:c.182T>A: p.V61D	-	-	-	het (0.375)	.	.	.	.	.	0.07, 0.93, T	0.735,P	1.000,1.00 0,D	0.15	0.0110 99107	24.6
ZFAND4	NM_001128324: ex5:c.371A>C: p.D124A	-	-	-	het (0.228)	.	.	.	.	.	0, 1.00, D	0.738,P	1.000,1.00 0,D	0.273	0.0592 79456	26.6
APLNR	NM_005161: ex1:c.1043C>T: p.S348L	het (0.323)	-	-	-	.	rs369393 051	3.77E-05	3.23E-05	.	0.26, 0.74, T	0.773,P	1.000,1.00 0,D	0.183	0.0232 65523	31
ANO2	NM_001278596: ex22:c.2375C>T: p.P792L NM_001278597: ex22:c.2363C>T: p.P788L	-	het (0.358)	-	-	.	rs370114 605	1.90E-05	.	.	0.05, 0.95, D	1.0,D	1,1.0,D	0.629	0.1251 83679	27.4
TDRD9	NM_153046: ex1:c.181C>T: p.Q61X	het (0.391)	-	-	-	.	.	.	.	.	.	.	.	.	.	27.2
NF2	NM_000268: ex3:c.331C>T: p.Q111X	-	het (0.708)	-	-	.	.	.	.	COSM22 268	.	.	1,1.0,D	.	.	40
PDE6A	NM_000440: ex18:c.2161C>T: p.L721F	-	-	het (0.425)	-	.	.	.	.	.	0, 1.00, D	0.836,P	1.000,1.00 0,D	0.782	0.0720 14929	28.1
DROSHA	NM_013235: ex19:c.2570G>A: p.C857Y	het (0.315)	-	-	-	.	.	.	.	.	0, 1.00, D	0.706,P	1,1.0,D	0.351	0.0305 23992	32
DST	NM_015548: ex84:c.15485C>T: p.A5162V	-	-	-	het (0.332)	.	.	.	.	.	0.02, 0.98, D	0.889,P		0.119	0.0045 07108	24.1

* Minor allele frequency (MAF) in Non-TCGA ExAC (The Exome Aggregation Consortium; http://exac.broadinstitute.org/), gnomaD (http://gnomad.broadinstitute.org/).

** Functional impact prediction results of 6 bioinformatics algorithms. The Revel score changes between 0 to 1 and more damaging variants have higher scores. CADD score ≥20 indicates deleterious variants.

*** Positive staining means that there was no alteration to the *SMARCB1* gene. Negative staining means that there is an alteration to the *SMARCB1* gene affecting protein expression.

Supplementary Table 5. Somatic mutations found by WES in the choroid plexus papilloma from individual III-1

Gene	Gene Info	III-1 CPP (VAF)	rsID138	ExacNoTCGA_MAF*	gnomad MAF*	COSMIC_ID	SIFT**	Polyphen2**	Mutation Taster**	Revel**	MCAP**	CADD_phred**
PRPF3	NM_004698: ex7:c.856C>T p.R286C	het (0.11)	.	.	.	.	0,1.00,D	0.98,D	1,1.0,D	0.655	0.315	34
ERCC6	NM_000124: ex18c.3662G>A: p.R1221Q	het (0.13)	rs200431100	1.88E-05	3.23E-05	COSM918653	0.1,0.90,T	0.926,D	1,1.0,D	0.497	0.062	35
FAM111B	NM_198947: ex4:c.G689G>A: p.R230H	het (0.11)	.	2.83E-05	3.24E-05	.	0,1.00,D	0.857,P	1,0.0,N	0.307	0.053	24.3
CTSW	NM_001335: ex7:c.739G>A: p.E247K	het (0.13)				.	0,1.00,D	0.9,P	1.000,0.000,N	0.689	0.090	24.6
LRFN5	NM_152447: ex4:c.1877C>T: p.T626I	het (0.29)	.	.	.	COSM401477	0.25,0.75,T	0.247,B	1,1.0,D	0.197	0.015	24.9
PROX2	NM_001080408: ex3:c.962C>T: p.T321M	het (0.12)	.	.	.	.	0,1.00,D	1.0,D	1,1.0,D	0.658	0.117	33
TMOD2	NM_001142885: ex5:c.421C>T: p.H141Y, NM_014548: ex5:c.421C>T: p.H141Y	het (0.11)	rs141909319	2.83E-05	3.23E-05	.	0.42,0.58,T	0.935,D	1.000,1.000,D	0.27	0.007	23.2
TEKT5	NM_144674: ex4:c.727C>T: p.R243W	het (0.13)	rs141029189	3.78E-05	6.47E-05	.	0,1.00,D	0.996,D	1.000,1.000,D	0.316	0.044	29.1
ABHD8	NM_024527: ex2:c.439C>T: p.R147W	het (0.17)	.	.	.	.	0.04,0.96,D	0.548,P	0.991,0.009,N	0.088	0.108	28.8

Gene	Gene Info	III-1 CPP (VAF)	rsID138	ExacNoTCGA_MAF*	gnomad MAF*	COSMIC_ID	SIFT**	Polyphen2**	Mutation Taster**	Revel**	MCAP**	CADD_phred**
NXPH2	NM_007226: ex2:c.263C>T: p.T88M	het (0.14)	.	.	.	.	.	0.984,D	1.000,1.000,D	0.263	0.010	27.9
ARFIP1	NM_014447: ex7:c.716G>A: p.R239H	het (0.15)	.	.	3.23E-05	COSM1052172, COSM1052173	0.1,0.90,T	1.0,D	1,1.0,D	0.786	0.112	34
P4HA2	NM_001142599: ex3:c.82+5G>A, NM_001017974: ex2:c.82+5G>A	het (0.14)	.	9.63E-06	.	.	.	.	.	.	.	.
COL12A1	NM_080645: ex20:c.2401C>T: p.R801C, NM_004370: ex35:c.5893C>T: p.R1965C	het (0.15)	rs200487396	1.00E-04	1.00E-04	COSM229731	0,1.00,D	0.976,D	1.000,1.000,D	0.811	0.080	23.6
NUDCD3	NM_015332: ex5:c.975+5G>A	het (0.13)	.	.	.	.	.	.	.	.	.	.
RCAN3	NM_001251984: ex4:c.211G>A:p.V71M	het (0.13)	rs201305577	.	3.23E-05	.	0,1.00,D	1.0,D	1,1.0,D	0.484	0.102	33
ACP2	NM_001610:ex4:c.314C>T: p.T105I	het (0.10)	.	.	.	.	0,1.00,D	1.0,D	1,1.0,D	0.715	0.043	29.5
STRN3	NM_014574: ex9:c.1147C>T: p.R383X, NM_001083893: ex11:c.1399C>T: p.R467X	het (0.19)	.	.	.	COSM3419762, COSM3419763	.	.	.	.	.	39
CHD3	NM_001005271: ex1:c.219_220insCCG: p.F73delinsFP	het (0.57)	.	.	0.0119	.	.	.	.	.	.	.

Gene	Gene Info	III-1 CPP (VAF)	rsID138	ExacNoTCGA_MAF*	gnomad MAF*	COSMIC_ID	SIFT**	Polyphen2**	Mutation Taster**	Revel**	MCAP**	CADD_phred**
ARHGAP40	NM_001164431: ex2:c.337+5G>A	het (0.14)	.	.	.	.	.	.	.	.	.	.
MST1	NM_020998: ex15:c.1640G>T: p.G547V	het (0.16)	.	.	.	.	0.17,0.83,T	1.0,D	1,1.0,D	0.727	0.140	25.8
PDLIM5	NM_001256428: ex5:c.370C>T: p.R124C	het (0.11)	rs201891054	3.77E-05	6.51E-05	COSM1431851, COSM1431852	0.17,0.83,T	0.764,P	0.963,0.963,D	0.066	0.019	24.4
MRRF	NM_199177: ex5:c.587G>A: p.W196X	het (0.11)	.	.	.	.	.	.	.	.	.	11.41
MLXIP	NM_014938: ex6:c.902G>A: p.R301Q	het (0.15)	.	.	.	.	0.11,0.89,T	0.99,D	1,1.0,D	0.158	0.022	32
RHPN2	NM_033103: ex3:c.217G>A: p.V73M	het (0.10)	.	9.00E-04	.	.	0,1.00,D	0.984,D	1,1.0,D	0.334	0.075	26.9

* Minor allele frequency (MAF) in Non-TCGA ExAC (The Exome Aggregation Consortium; http://exac.broadinstitute.org/), gnomaAD (http://gnomad.broadinstitute.org/).
** Functional impact prediction results of 6 bioinformatics algorithms. The Revel score changes between 0 to 1 and more damaging variants have higher scores. CADD score ≥ 20 indicates deleterious variants.

Supplementary Table 6. Coverage results for the WES experiment in the 6 tumors (4 schwannomas from individual II-2, 1 schwannoma from individual I-1 and 1 CPP from III-1)

Sample_id	Mean	%CCDS bases ≥ 5x coverage	%CCDS bases ≥ 10x coverage	%CCDS bases ≥ 20x coverage	%CCDS bases ≥ 50x coverage
II-2-Schw1	136	98.3	98.0	97.4	92.3
II-2-Schw2	196	98.4	98.2	97.9	95.9
II-2-Schw3	194	98.4	98.2	97.9	95.7
II-2-Schw4	187	98.4	98.2	97.8	95.2
III-1-CPP	93	96.4	93.9	88.8	70.1
I-1-Schw	292.95	98.4	98.1	97.5	94.6

Supplementary Table 7. Summary of the Sequencing Methods for all Tumors and blood from MNG patients

DGCR8 screening	Number of samples				
	CPTs	Schwannomas	MNGs (germline)	Benign Thyroid nodules	PTC
Fluidigm	50	56*	7	NA	NA
Haloplex[HS]	NA	61**	1	NA	NA
WES	24	NA	4***	NA	NA
Sanger sequencing Full Gene	NA	64	6	NA	NA
Sanger sequencing E518K	NA	NA	NA	106	315
Total	**74**	**181**	**18**	**106**	**315**

* 11 cases were sequenced by Fluidigm in parallel with the Haloplex[HS] experiment.** 11 cases were also sequenced using the Fluidigm assay to test the capture results from the Haloplex[HS] experiment. NA : not done; CPTs; Choroid plexus tumors; MNGs: Multinodular goiters. *** only probands are included; PTC: Papillary thyroid cancers.

Supplementary Table 8. *DGCR8* **Sequencing Summary of** *DGCR8* **(NM_022720) for all sporadic CPTs and schwannomas**

Sample ID	TUMOR TYPE	Variant	Predictors					MAF		Sequencing method
			PPH2	SIFT	PROVEAN	Mutation Assessor	CADD	gnomAD	1000 Genomes	
CPT438*	WHO-III (CPC)	c.1763A>G, p.(K588R)	0.985 (probably damaging)	0.13 (tolerated)	-0.695 (Neutral)	0.550 (neutral)	24.9	0.005920	0.0034	Fluidigm

* CPT438 has LOH

Sample ID	TUMOR TYPE	Variant	Predictors					MAF		Sequencing method
			PPH2	SIFT	PROVEAN	Mutation Assessor	CADD	gnomAD	1000 Genomes	
Schw42	Primary tumor	c.1763A>G, p.(K588R)	0.637 (probably damaging)	0.13 (tolerated)	-0.695 (Neutral)	0.550 (neutral)	24.9	0.005920	0.0034	Fluidigm
Schw62	Primary tumor	c.1763A>G, p.(K588R)	0.637 (probably damaging)	0.13 (tolerated)	-0.695 (Neutral)	0.550 (neutral)	24.9	0.005920	0.0034	Sanger
Schw66	Primary tumor	c.1147A>G, p.(S383G)	0.000 (benign)	0.514 (tolerated)	0.114 (Neutral)	0.345 (neutral)	14.29	N/A	N/A	Haloplex
Schw67	Recurrence of schw62	c.1763A>G, p.(K588R)	0.637 (probably damaging)	0.13 (tolerated)	-0.695 (Neutral)	0.550 (neutral)	24.9	0.005920	0.0034	Haloplex
Schw137	Primary tumor	c.1763A>G, p.(K588R)	0.637 (probably damaging)	0.13 (tolerated)	-0.695 (Neutral)	0.550 (neutral)	24.9	0.005920	0.0034	Sanger
Schw164*	Multiple tumors	c.1763A>G, p.(K588R)	0.637 (probably damaging)	0.13 (tolerated)	-0.695 (Neutral)	0.550 (neutral)	24.9	0.005920	0.0034	Sanger
Schw165*	Multiple tumors	c.1763A>G, p.(K588R)	0.637 (probably damaging)	0.13 (tolerated)	-0.695 (Neutral)	0.550 (neutral)	24.9	0.005920	0.0034	Sanger

* Schw164 and schw165 are from the same patient, which suggests the variant c.1763A>G;p.K588R is a germline variant. **DGCR8 MNGs series:** No variant in *DGCR8* was found in germline DNA from the 18 MNG cases with a suspected hereditary origin.

Supplementary Table 9. Differentially expressed miRNAs in DGCR8 mutated vs DGCR8 wild type schwanomas

ID	Name	logFC	AveExpr	t	P.Value	adj.P.Val
MIMAT0004550	hsa-miR-30c-2-3p	-3.60	7.11	-12.93	7.27E-08	2.94E-05
MIMAT0003885	hsa-miR-454-3p	-3.53	5.47	-12.67	8.91E-08	2.94E-05
MIMAT0000222	hsa-miR-192-5p	-3.57	6.92	-12.62	9.32E-08	2.94E-05
MIMAT0000275	hsa-miR-218-5p	-3.39	9.51	-11.68	2.03E-07	3.60E-05
MIMAT0004956	hsa-miR-374b-3p	-3.33	3.08	-10.71	4.77E-07	5.68E-05
MIMAT0000244	hsa-miR-30c-5p	-2.09	11.78	-10.58	5.39E-07	5.68E-05
MIMAT0003249	hsa-miR-584-5p	-5.37	5.78	-10.18	7.83E-07	6.76E-05
MIMAT0004810	hsa-miR-629-5p	-3.55	6.67	-9.60	1.39E-06	9.55E-05
MIMAT0013517	hsa-miR-2682-5p	-7.43	0.54	-9.58	1.41E-06	9.55E-05
MIMAT0004505	hsa-miR-32-3p	-3.40	2.83	-9.50	1.54E-06	9.74E-05
MIMAT0000460_1	hsa-miR-194-5p	-2.18	5.85	-9.09	2.35E-06	1.07E-04
MIMAT0000772	hsa-miR-345-5p	-2.29	5.99	-8.98	2.64E-06	1.07E-04
MIMAT0019047	hsa-miR-4510	-3.83	1.34	-8.97	2.67E-06	1.07E-04
MIMAT0003886	hsa-miR-769-5p	-2.05	7.29	-8.90	2.88E-06	1.07E-04
MIMAT0005825	hsa-miR-1180-3p	-2.90	5.37	-8.78	3.27E-06	1.07E-04
MIMAT0004784	hsa-miR-455-3p	-3.80	5.34	-8.76	3.33E-06	1.07E-04
MIMAT0000692	hsa-miR-30e-5p	-2.50	10.53	-8.74	3.42E-06	1.07E-04
MIMAT0005796	hsa-miR-1271-5p	-2.96	4.82	-8.49	4.49E-06	1.14E-04
MIMAT0004565	hsa-miR-218-1-3p	-3.99	1.09	-8.44	4.74E-06	1.15E-04
MIMAT0004955	hsa-miR-374b-5p	-3.21	7.82	-8.30	5.54E-06	1.28E-04
MIMAT0018443	hsa-miR-374c-5p	-4.46	-0.05	-8.26	5.79E-06	1.28E-04
MIMAT0000693	hsa-miR-30e-3p	-1.86	8.75	-8.18	6.34E-06	1.29E-04
MIMAT0000090	hsa-miR-32-5p	-3.48	6.80	-8.06	7.32E-06	1.36E-04
MIMAT0004486	hsa-let-7f-1-3p	-2.80	3.49	-8.01	7.72E-06	1.38E-04
MIMAT0022706	hsa-miR-561-5p	-4.45	-0.69	-8.01	7.73E-06	1.38E-04
MIMAT0027663	hsa-miR-6881-3p	4.40	1.51	11.54	2.28E-07	3.60E-05
MIMAT0030417	hsa-miR-6516-5p	3.89	2.67	10.18	7.86E-07	6.76E-05
MIMAT0019859	hsa-miR-4734	4.74	-1.45	9.75	1.20E-06	9.45E-05
MIMAT0027632	hsa-miR-6866-5p	2.66	1.93	9.23	2.03E-06	1.07E-04
MIMAT0004515	hsa-miR-29b-2-5p	2.83	6.55	9.12	2.26E-06	1.07E-04
MIMAT0018997	hsa-miR-4470	3.17	2.11	9.07	2.39E-06	1.07E-04
MIMAT0025852	hsa-miR-6721-5p	3.64	0.04	8.95	2.73E-06	1.07E-04
MIMAT0005584	hsa-miR-1229-3p	3.81	1.46	8.77	3.29E-06	1.07E-04
MIMAT0025479	hsa-miR-6511a-3p	2.56	2.84	8.68	3.63E-06	1.07E-04
MIMAT0005911	hsa-miR-1260a	3.52	4.44	8.65	3.76E-06	1.08E-04
MIMAT0004950	hsa-miR-877-3p	4.31	1.90	8.54	4.24E-06	1.14E-04
MIMAT0000080	hsa-miR-24-3p	1.71	14.08	8.53	4.29E-06	1.14E-04
MIMAT0005591	hsa-miR-1236-3p	3.78	-1.17	8.47	4.56E-06	1.14E-04
MIMAT0027573	hsa-miR-6780b-3p	4.22	-1.09	8.32	5.39E-06	1.28E-04
MIMAT0025845	hsa-miR-6716-3p	3.16	3.02	8.28	5.66E-06	1.28E-04

ID	Name	logFC	AveExpr	t	P.Value	adj.P.Val
MIMAT0027645	hsa-miR-6872-3p	3.21	-0.25	8.22	6.10E-06	1.29E-04
MIMAT0015041	hsa-miR-1260b	3.77	5.13	8.20	6.23E-06	1.29E-04
MIMAT0002808	hsa-miR-511-5p	3.90	3.60	8.15	6.55E-06	1.29E-04
MIMAT0004693	hsa-miR-330-5p	2.57	5.94	8.10	6.99E-06	1.33E-04
MIMAT0019873	hsa-miR-4742-3p	2.94	0.92	8.09	7.02E-06	1.33E-04
MIMAT0000273	hsa-miR-216a-5p	6.56	-1.06	7.94	8.40E-06	1.47E-04
MIMAT0005580	hsa-miR-1227-3p	3.66	0.95	7.83	9.50E-06	1.64E-04
MIMAT0025848	hsa-miR-6511b-3p	2.35	2.99	7.68	1.14E-05	1.90E-04
MIMAT0027554	hsa-miR-6827-5p	2.97	0.28	7.63	1.21E-05	1.96E-04
MIMAT0027567	hsa-miR-6833-3p	2.62	1.10	7.62	1.22E-05	1.96E-04

Top 25 over- and under- expressed miRNA (blue and red respectively) from differential miRNA expression analysis between Schwannoma cases with and without *DGCR8* mutation (n total = 9), corresponding to the volcano plot shown in Figure 4B of the manuscript. logFC: log2 of Fold Change;AveExpr: normalized Average Expression across all samples; t: moderated t-statistics; FDR: False Discovery Rate.

Supplementary Table 10. Differentially expressed mRNAs in DGCR8 mutated vs DGCR8 wild type schwanomas

GeneNam	EnsID	logFC	AveExp	T	P.Value	FDR
KRAS	ENSG00000133703	1.40	6.77	12.93	3.03E-07	1.27E-03
FAM102B	ENSG00000162636	1.29	5.92	9.00	6.90E-06	4.70E-03
SNN	ENSG00000184602	0.78	6.63	8.97	7.11E-06	4.70E-03
TMEM139	ENSG00000178826	3.06	2.79	8.85	7.98E-06	4.70E-03
SIGMAR1	ENSG00000147955	1.19	5.43	8.41	1.22E-05	5.75E-03
RAP2C	ENSG00000123728	0.86	5.64	7.93	1.98E-05	5.89E-03
ERGIC2	ENSG00000087502	1.24	6.56	7.78	2.31E-05	5.89E-03
NRAS	ENSG00000213281	1.10	6.27	7.74	2.42E-05	5.89E-03
L1TD1	ENSG00000240563	2.94	3.68	7.75	2.39E-05	5.89E-03
CNEP1R1	ENSG00000205423	0.66	4.46	7.59	2.83E-05	5.94E-03
TGIF2	ENSG00000118707	0.70	5.30	7.58	2.88E-05	5.94E-03
COMMD3	ENSG00000148444	0.79	4.19	7.53	3.03E-05	5.94E-03
CBR3	ENSG00000159231	0.83	3.89	7.22	4.24E-05	7.14E-03
CDC23	ENSG00000094880	0.95	5.13	7.13	4.65E-05	7.46E-03
PLK2	ENSG00000145632	2.07	7.46	7.08	4.98E-05	7.46E-03
RBM3	ENSG00000102317	0.97	7.81	7.05	5.10E-05	7.46E-03
MYL12B	ENSG00000118680	0.93	7.28	7.04	5.17E-05	7.46E-03
CDC42	ENSG00000070831	0.90	7.98	6.92	5.96E-05	8.42E-03
RAP2B	ENSG00000181467	1.02	6.50	6.63	8.26E-05	9.05E-03
FLJ27365	ENSG00000197182	1.97	6.46	6.39	1.11E-04	1.09E-02
SPCS3	ENSG00000129128	0.70	7.25	6.27	1.28E-04	1.21E-02
TMEM33	ENSG00000109133	0.68	6.99	6.25	1.31E-04	1.22E-02
DUSP12	ENSG00000081721	0.77	4.15	6.19	1.42E-04	1.25E-02
METRNL	ENSG00000176845	1.10	6.72	6.15	1.49E-04	1.25E-02
CCDC50	ENSG00000152492	0.68	7.29	6.09	1.61E-04	1.25E-02
ZBTB16	ENSG00000109906	-3.12	6.41	-12.15	5.24E-07	1.27E-03

GeneNam	EnsID	logFC	AveExp	T	P.Value	FDR
ATAD3B	ENSG00000160072	-1.48	4.21	-11.47	8.65E-07	1.53E-03
GBP3	ENSG00000117226	-2.07	5.18	-11.04	1.21E-06	1.71E-03
GPR83	ENSG00000123901	-5.05	3.85	-12.11	5.38E-07	1.27E-03
SAFB2	ENSG00000130254	-1.29	6.05	-10.45	1.94E-06	2.28E-03
SEC14L1	ENSG00000129657	-1.72	7.40	-9.32	5.14E-06	4.70E-03
KCNJ2	ENSG00000123700	-1.44	3.37	-9.09	6.34E-06	4.70E-03
SERPINA5	ENSG00000188488	-2.68	6.23	-8.88	7.75E-06	4.70E-03
ECHDC2	ENSG00000121310	-2.16	5.43	-8.66	9.52E-06	4.80E-03
ZFAND5	ENSG00000107372	-2.29	9.25	-8.67	9.47E-06	4.80E-03
NEK9	ENSG00000119638	-0.76	6.88	-8.30	1.36E-05	5.81E-03
FKBP5	ENSG00000096060	-2.58	8.41	-8.27	1.40E-05	5.81E-03
TSC22D3	ENSG00000157514	-1.94	8.16	-8.19	1.52E-05	5.89E-03
BEX4	ENSG00000102409	-1.70	4.72	-7.94	1.95E-05	5.89E-03
NBPF14	ENSG00000122497	-3.39	3.93	-7.95	1.94E-05	5.89E-03
GCC2	ENSG00000135968	-0.72	6.81	-7.89	2.06E-05	5.89E-03
DCXR	ENSG00000169738	-1.17	3.40	-7.85	2.15E-05	5.89E-03
SULT1A1	ENSG00000196502	-3.15	3.34	-7.84	2.18E-05	5.89E-03
ZNF812	ENSG00000224689	-3.20	2.38	-7.81	2.23E-05	5.89E-03
ZDBF2	ENSG00000204186	-1.62	4.94	-7.58	2.86E-05	5.94E-03
OLR1	ENSG00000173391	-2.97	4.81	-7.55	2.95E-05	5.94E-03
CEBPB	ENSG00000172216	-1.78	6.04	-7.57	2.89E-05	5.94E-03
PDK4	ENSG00000004799	-2.36	9.09	-7.54	2.99E-05	5.94E-03
BAIAP2	ENSG00000175866	-1.90	5.50	-7.45	3.30E-05	6.31E-03
VMP1	ENSG00000062716	-2.00	8.74	-7.38	3.54E-05	6.58E-03

Top 25 over- and under-expressed mRNA (red and blue respectively) from differential mRNA expression analysis between Schwannoma cases with and without *DGCR8* mutation (n total = 9), corresponding to the volcano plot shown in Figure 4A of the manuscript. logFC log2 of Fold Change; AveExpr corresponds to normalized Average Expression across all samples; t = moderated t-statistics; FDR False Discovery Rate.

Supplementary Table 11. Differentially expressed miRNAs in DGCR8 mutated vs DGCR8 wild type Wilms Tumors

ID	Name	logFC	AveExpr	t	P.Value	FDR
MIMAT0000772	hsa-miR-345-5p	-4.38	3.89	-10.63	4.27E-11	2.74E-08
MIMAT0000692	hsa-miR-30e-5p	-2.47	11.72	-9.06	1.23E-09	2.62E-07
MIMAT0003322	hsa-miR-652-3p	-2.51	4.18	-8.50	4.40E-09	7.06E-07
MIMAT0000693	hsa-miR-30e-3p	-2.60	11.58	-8.29	7.27E-09	8.96E-07
MIMAT0004955	hsa-miR-374b-5p	-2.79	4.99	-7.98	1.52E-08	1.22E-06
MIMAT0002876	hsa-miR-505-3p	-2.89	4.74	-7.48	5.10E-08	2.04E-06
MIMAT0004680	hsa-miR-130b-5p	-4.44	5.29	-7.45	5.44E-08	2.05E-06
MIMAT0003885	hsa-miR-454-3p	-2.84	4.39	-7.30	7.99E-08	2.69E-06
MIMAT0004697	hsa-miR-151a-5p	-2.07	6.96	-7.12	1.25E-07	3.96E-06
MIMAT0000257_1	hsa-miR-181b-5p	-2.81	9.91	-6.88	2.27E-07	6.61E-06
MIMAT0022726	hsa-miR-1306-5p	-3.49	2.57	-6.75	3.16E-07	8.45E-06

ID	Name	logFC	AveExpr	t	P.Value	FDR
MIMAT0005794	hsa-miR-1296-5p	-3.30	3.90	-6.68	3.74E-07	9.60E-06
MIMAT0004911	hsa-miR-874-3p	-2.66	4.75	-6.56	5.17E-07	1.27E-05
MIMAT0003218	hsa-miR-92b-3p	-2.71	6.60	-6.33	9.43E-07	1.75E-05
MIMAT0001080	hsa-miR-196b-5p	-3.39	11.40	-6.31	9.85E-07	1.75E-05
MIMAT0000222	hsa-miR-192-5p	-3.03	7.30	-6.28	1.07E-06	1.79E-05
MIMAT0004502	hsa-miR-28-3p	-2.08	10.38	-6.27	1.09E-06	1.79E-05
MIMAT0000447	hsa-miR-134-5p	-3.02	7.76	-6.16	1.44E-06	2.20E-05
MIMAT0000754	hsa-miR-337-3p	-2.44	5.14	-5.93	2.67E-06	3.81E-05
MIMAT0000090	hsa-miR-32-5p	-2.17	3.91	-5.82	3.50E-06	4.78E-05
MIMAT0000758	hsa-miR-135b-5p	-3.86	5.15	-5.79	3.80E-06	5.08E-05
MIMAT0003258	hsa-miR-590-5p	-2.90	2.64	-5.76	4.15E-06	5.29E-05
MIMAT0006789	hsa-miR-1468-5p	-3.54	2.29	-5.75	4.29E-06	5.29E-05
MIMAT0005920	hsa-miR-1266-5p	-3.13	2.09	-5.75	4.29E-06	5.29E-05
MIMAT0019208	hsa-miR-3074-5p	-4.26	2.26	-5.70	4.89E-06	5.91E-05
MIMAT0005584	hsa-miR-1229-3p	4.46	0.69	9.31	7.14E-10	2.29E-07
MIMAT0030020	hsa-miR-7705	3.67	-1.10	8.23	8.39E-09	8.96E-07
MIMAT0004515	hsa-miR-29b-2-5p	3.14	2.76	8.15	1.01E-08	9.26E-07
MIMAT0027577	hsa-miR-6837-3p	3.26	-0.26	7.89	1.90E-08	1.35E-06
MIMAT0027410	hsa-miR-6755-5p	3.51	-0.57	7.80	2.34E-08	1.50E-06
MIMAT0005949	hsa-miR-664a-3p	2.97	3.59	7.70	2.96E-08	1.72E-06
MIMAT0027513	hsa-miR-6806-3p	2.17	1.23	7.67	3.23E-08	1.72E-06
MIMAT0019845	hsa-miR-4726-5p	3.24	-0.58	7.59	3.92E-08	1.92E-06
MIMAT0027691	hsa-miR-6895-3p	3.91	-1.61	7.55	4.26E-08	1.92E-06
MIMAT0018001	hsa-miR-3620-3p	3.83	-0.18	7.53	4.50E-08	1.92E-06
MIMAT0000751	hsa-miR-330-3p	2.79	0.83	7.42	5.98E-08	2.13E-06
MIMAT0018186	hsa-miR-3912-3p	2.78	0.67	7.10	1.30E-07	3.96E-06
MIMAT0022272	hsa-miR-664b-3p	2.81	-0.08	6.43	7.19E-07	1.66E-05
MIMAT0004949	hsa-miR-877-5p	2.94	2.91	6.42	7.37E-07	1.66E-05
MIMAT0025845	hsa-miR-6716-3p	3.13	-1.25	6.41	7.58E-07	1.66E-05
MIMAT0005577	hsa-miR-1226-3p	3.57	4.12	6.40	7.79E-07	1.66E-05
MIMAT0019873	hsa-miR-4742-3p	2.98	0.37	6.36	8.56E-07	1.75E-05
MIMAT0000443	hsa-miR-125a-5p	1.81	10.09	6.31	9.75E-07	1.75E-05
MIMAT0018962	hsa-miR-4444	2.25	-0.45	6.31	9.80E-07	1.75E-05
MIMAT0005948	hsa-miR-664a-5p	2.87	0.97	6.29	1.03E-06	1.79E-05
MIMAT0004921	hsa-miR-889-3p	2.89	4.69	6.25	1.14E-06	1.82E-05
MIMAT0000753	hsa-miR-342-3p	2.09	7.99	6.22	1.23E-06	1.92E-05
MIMAT0027677	hsa-miR-6888-3p	2.85	-1.37	6.13	1.55E-06	2.32E-05
MIMAT0002174	hsa-miR-484	1.92	6.65	6.03	2.05E-06	2.98E-05
MIMAT0015050	hsa-miR-323b-3p	3.56	2.62	5.89	2.95E-06	4.11E-05

Top 25 over- and under- expressed miRNA (blue and red respectively) from differential miRNA expression analysis between Wilms Tumor cases with and without *DGCR8* mutation (n total = 24), corresponding to the volcano plot shown in Figure 4C of the manuscript. logFC: log2 of Fold Change;AveExpr: normalized Average Expression across all samples; t: moderated t-statistics; FDR: False Discovery Rate.

Supplementary Table 12. Proportions of mirtrons within the total miRNA populations in DGCR8 or DICER1 mutated tumors compared to their wild types counterparts

Experiment	Total miRNAs expressed	Total mirtrons expressed	Higher in the mutant samples (FDR < 0.01)	Lower in the mutant samples (FDR< 0.01)
DGCR8	871	139 (16%)	113 (81%)	0 (0%)
DICER1	825	60 (7%)	8 (13%)	5 (8%)

The percentage of mirtrons with higher/lower expression values (FDR < 0.01) in DGCR8 mutated schwannomas compared to wild types (Figure 4B; n sample = 9) and DICER1-mutated pituitary blastomas compared to DICER1 wild type (Supplementary Figure 14; n sample = 10). The data corresponds to the black dots in the corresponding figures.

Supplementary Table 13. Hallmark gene set enrichment analysis for differentially expressed transcripts in DGCR8 mutated vs DGCR8 wild type schwannomas

NAME	SIZE	ES	NES	FDR
HALLMARK_MYC_TARGETS_V1	169	0.407191	2.096808	4.86E-04
HALLMARK_INTERFERON_GAMMA_RESPONSE	121	-0.45651	-2.08793	0.001321
HALLMARK_TNFA_SIGNALING_VIA_NFKB	127	-0.44627	-2.05127	7.62E-04
HALLMARK_INTERFERON_ALPHA_RESPONSE	66	-0.46511	-1.91045	0.00307
HALLMARK_KRAS_SIGNALING_DN	34	-0.53137	-1.90191	0.002496

SIZE: number of genes in the gene set; ES: Enrichment score; NES: Normalized Enrichment Score across gene sets; FDR; False Discovery Rate.

Supplementary Table 14. Primers used for amplification and sequencing of *DGCR8* gene in DNA of FFPE samples. cDNA-specific primers for amplification and sequencing of the E518K variant in cDNA are included at the bottom of the table

PRIMERS	Exon	SEQUENCE (5'-->3')
DGCR8-1-1-s	1	GCT GTG TAG ATT TAT GTG AGG GC
DGCR8-1-1-as	1	ACT GTC CAT CAC CAC CAG AG
DGCR8-1-2-s	1	GAG CTC GCC CCT TCC AAG
DGCR8-1-2-as	1	AGC AAC TTA AGG TCA GGG GA
DGCR8-1-3-s	1	TAG ACC CGA ACT GTA GTG GC
DGCR8-1-3-as	1	CAA CAC TCC CGC CAA AGG
DGCR8-1-4-s	1	GTG GGG ACG TGC ATG CTT
DGCR8-1-4-as	1	GCT GCA ATT CCC AAA TCT CTC TT
DGCR8-2-s	2	TGC TGT TGA GCT CTC CTG TT
DGCR8-2-as	2	GGC ACC AGA GCT CTC TCA AA
DGCR8-3-s	3	GGA TGT TCT TGT CTT CCT GTG C
DGCR8-3-as	3	CAT GTG TGT GGA TGT GCA CG
DGCR8-4-1-s	4	GGA GGC ATC AGT CGT GAC TT
DGCR8-4-1-as	4	TTG ACG GGG GAC ACA TCC
DGCR8-4-2-s	4	GGA GCA AAG CAG TGA CCT CA
DGCR8-4-2-as	4	TCA TGG GTC CCA GGA GGC
DGCR8-5-s	5	GTT TCT CTG GTA AAT CTG GGA CA
DGCR8-5-as	5	CAT GCC CTC AAC ACA TCA CA
DGCR8-6-s	6	GCC CCT AGT TAC TGA CAT GGT
DGCR8-6-as	6	CCC TGA CCA AAG TTA CAC CT
DGCR8-7-s	7	GAC TGT GCA CAC GCT TTT GA
DGCR8-7-as	7	CCA CTT GTC ACC ACT GCT CA
DGCR8-8-s	8	ACA GTT CAC TCT GCA GGG TG
DGCR8-8-as	8	CAG CTC ACA CTA ACA GGG CA
DGCR8-9-s	9	GTG GGG ACT CAC AAG CCT C
DGCR8-9-as	9	TGG GAC AAA CAG CCA CAA GA
DGCR8-10-s	10	AGA GCA GGC CTC CTC AGA G
DGCR8-10-as	10	CTG AGA CCA AGC CAC AGA GG
DGCR8-11-s	11	TGT GGG TCA GGA GGG CTG
DGCR8-11-as	11	AGA GCC TCA GGA ATA CGC TC
DGCR8-12-s	12	CTA CAG CCT GCA GTC CTG AG
DGCR8-12-as	13	ACA GGT GCC ACA GGA ATG G
DGCR8-13-s	13	CCT CCA CCT TGT GTC TTC CC
DGCR8-13-as	13	CTG GTC TCC TCA GAA GTG CG
cDNA-DGCR8-518-S	6-7 cDNA	TTG CCA GCC AAT CAG AAG C
cDNA-DGCR8-518-AS	6-7 cDNA	AAG TCA GGG ATG AGG ATT TCC

References:
1. Rudkin TM, Hamel N, Galvez M, Hogervorst F, Gille JJ, Moller P, et al. The frequent BRCA1 mutation 1135insA has multiple origins: a haplotype study in different populations. *BMC Med Genet.* 2006;7:15.
2. Sabbaghian N, Srivastava A, Hamel N, Plourde F, Gajtko-Metera M, Niedziela M, et al. Germ-line deletion in DICER1 revealed by a novel MLPA assay using synthetic oligonucleotides. *Eur J Hum Genet.* 2014;22(4):564-7.
3. de Kock L, Sabbaghian N, Druker H, Weber E, Hamel N, Miller S, et al. Germ-line and somatic DICER1 mutations in pineoblastoma. *Acta Neuropathol.* 2014;128(4):583-95.
4. Rivera BF, S; Rabinowicz, S; Watters, AK; Leventer, R; Levental, M; Khanna, M; Foulkes WD. SMO Syndrome: A Unifying Molecular Diagnosis That Suggests Therapeutic Opportunities. *JCO Precision Oncology:* 2, 1-6, 2018.
5. Wang K, Li M, and Hakonarson H. ANNOVAR: functional annotation of genetic variants from high-throughput sequencing data. *Nucleic Acids Res.* 2010;38(16):e164.
6. Schwarz JM, Rodelsperger C, Schuelke M, and Seelow D. MutationTaster evaluates disease-causing potential of sequence alterations. *Nat Methods.* 2010;7(8):575-6.
7. Kircher M, Witten DM, Jain P, O'Roak BJ, Cooper GM, and Shendure J. A general framework for estimating the relative pathogenicity of human genetic variants. *Nat Genet.* 2014;46(3):310-5.
8. Jagadeesh KA, Wenger AM, Berger MJ, Guturu H, Stenson PD, Cooper DN, et al. M-CAP eliminates a majority of variants of uncertain significance in clinical exomes at high sensitivity. *Nat Genet.* 2016;48(12):1581-6.
9. Rentzsch P, Witten D, Cooper GM, Shendure J, and Kircher M. CADD: predicting the deleteriousness of variants throughout the human genome. *Nucleic Acids Res.* 2019;47(D1):D886-D94.
10. Kumar P, Henikoff S, and Ng PC. Predicting the effects of coding non-synonymous variants on protein function using the SIFT algorithm. *Nat Protoc.* 2009;4(7):1073-81.
11. Adzhubei IA, Schmidt S, Peshkin L, Ramensky VE, Gerasimova A, Bork P, et al. A method and server for predicting damaging missense mutations. *Nat Methods.* 2010;7(4):248-9.
12. Robinson JT, Thorvaldsdottir H, Winckler W, Guttman M, Lander ES, Getz G, et al. Integrative genomics viewer. *Nat Biotechnol.* 2011;29(1):24-6.
13. Martin M. Cutadapt removes adapter sequences from high-throughput sequencing reads. *EMBnet journal.* 2011;17(1):pp-10.
14. Andrews S. FastQC A Quality Control tool for High Throughput Sequence Data. *http://wwwbioinformaticsbabrahamacuk/projects/fastqc/.*
15. Langmead B, and Salzberg SL. Fast gapped-read alignment with Bowtie 2. *Nat Methods.* 2012;9(4):357-9.
16. Liao Y, Smyth GK, and Shi W. featureCounts: an efficient general purpose program for assigning sequence reads to genomic features. *Bioinformatics.* 2014;30(7):923-30.
17. Gentleman RC, Carey VJ, Bates DM, Bolstad B, Dettling M, Dudoit S, et al. Bioconductor: open software development for computational biology and bioinformatics. *Genome Biol.* 2004;5(10):R80.
18. Robinson MD, McCarthy DJ, and Smyth GK. edgeR: a Bioconductor package for differential expression analysis of digital gene expression data. *Bioinformatics.* 2010;26(1):139-40.
19. Ritchie ME, Phipson B, Wu D, Hu Y, Law CW, Shi W, et al. limma powers differential expression analyses for RNA-sequencing and microarray studies. *Nucleic Acids Res.* 2015;43(7):e47.
20. Law CW, Chen Y, Shi W, and Smyth GK. voom: Precision weights unlock linear model analysis tools for RNA-seq read counts. *Genome Biol.* 2014;15(2):R29.

21. Bolger AM, Lohse M, and Usadel B. Trimmomatic: a flexible trimmer for Illumina sequence data. *Bioinformatics.* 2014;30(15):2114-20.
22. Anders S, Pyl PT, and Huber W. HTSeq--a Python framework to work with high-throughput sequencing data. *Bioinformatics.* 2015;31(2):166-9.
23. Wilkerson MD, and Hayes DN. ConsensusClusterPlus: a class discovery tool with confidence assessments and item tracking. *Bioinformatics.* 2010;26(12):1572-3.
24. Subramanian A, Tamayo P, Mootha VK, Mukherjee S, Ebert BL, Gillette MA, et al. Gene set enrichment analysis: a knowledge-based approach for interpreting genome-wide expression profiles. *Proc Natl Acad Sci U S A.* 2005;102(43):15545-50.
25. Liberzon A, Birger C, Thorvaldsdottir H, Ghandi M, Mesirov JP, and Tamayo P. The Molecular Signatures Database (MSigDB) hallmark gene set collection. *Cell Syst.* 2015;1(6):417-25.
26. Whiffin N, Minikel E, Walsh R, O'Donnell-Luria AH, Karczewski K, Ing AY, et al. Using high-resolution variant frequencies to empower clinical genome interpretation. *Genet Med.* 2017;19(10):1151-8.

CARE Checklist (2013) of information to include when writing a case report

CARE case report guidelines

Topic	Item	Checklist item description	Reported on Page
Title	**1**	The words "case report" should be in the title along with the area of focus	N/A
Key Words	**2**	2 to 5 key words that identify areas covered in this case report.	2
Abstract	**3a**	Introduction—What is unique about this case? What does it add to the medical literature?	3
	3b	The main symptoms of the patient and the important clinical findings	3
	3c	The main diagnoses, therapeutics interventions, and outcomes	3
	3d	Conclusion—What are the main "take-away" lessons from this case?	3
Introduction	**4**	One or two paragraphs summarizing why this case is unique with references	5
Patient Information	**5a**	De-identified demographic information and other patient specific information	5 and Supplementary p3
	5b	Main concerns and symptoms of the patient	5 and Supplementary p3
	5c	Medical, family, and psychosocial history including relevant genetic information (also see timeline).	5 and Supplementary p3
	5d	Relevant past interventions and their outcomes	5 and Supplementary p3
Clinical Findings	**6**	Describe the relevant physical examination (PE) and other significant clinical findings.	5 and Supplementary p3
Timeline	**7**	Important information from the patient's history organized as a timeline	Figure 1 and Supplementary p3
Diagnostic Assessment	**8a**	Diagnostic methods (such as PE, laboratory testing, imaging, surveys).	5-7 and Supplementary 3,4,7 9
	8b	Diagnostic challenges (such as access, financial, or cultural)	N/A
	8c	Diagnostic reasoning including other diagnoses considered	5-7 and Supplementary 3,4,7 9
	8d	Prognostic characteristics (such as staging in oncology) where applicable	5-7 and Supplementary 3,4,7 9
Therapeutic Intervention	**9a**	Types of intervention (such as pharmacologic, surgical, preventive, self-care)	5-7 and Supplementary 3,4,7 9
	9b	Administration of intervention (such as dosage, strength, duration)	N/A
	9c	Changes in intervention (with rationale)	N/A
Follow-up and Outcomes	**10a**	Clinician and patient-assessed outcomes (when appropriate)	5-7 and Supplementary 3,4,7 9
	10b	Important follow-up diagnostic and other test results	5-7 and Supplementary 3,4,7 9
	10c	Intervention adherence and tolerability (How was this assessed?)	N/A
	10d	Adverse and unanticipated events	N/A
Discussion	**11a**	Discussion of the strengths and limitations in your approach to this case	10-14
	11b	Discussion of the relevant medical literature.	10-14
	11c	The rationale for conclusions (including assessment of possible causes)	10-14
	11d	The primary "take-away" lessons of this case report	13-14
Patient Perspective	**12**	When appropriate the patient should share their perspective on the treatments they received	N/A
Informed Consent	**13**	Did the patient give informed consent? Please provide if requested	Yes ☒ No ☐